



Article

Exploring the Relationships between Land Surface Temperature and Its Influencing Factors Using Multisource Spatial Big Data: A Case Study in Beijing, China

Xiaoxi Wang ¹, Yaojun Zhang ² and Danlin Yu ^{3,*}¹ School of Marxism, Putian University, Putian 351100, China² School of Applied Economics, Renmin University of China, Beijing 100872, China³ Department of Earth and Environmental Studies, Montclair State University, Montclair, NJ 07043, USA

* Correspondence: yud@mail.montclair.edu; Tel.: +1-973-655-4313; Fax: +1-973-655-4072

Abstract: A better understanding of the relationship between land surface temperature (LST) and its influencing factors is important to the livable, healthy, and sustainable development of cities. In this study, we focused on the potential effect of human daily activities on LST from a short-term perspective. Beijing was selected as a case city, and Weibo check-in data were employed to measure the intensity of human daily activities. MODIS data were analyzed and used for urban LST measurement. We adopted spatial autocorrelation analysis, Pearson correlation analysis, and spatial autoregressive model to explore the influence mechanism of LST, and the study was performed at both the pixel scale and subdistrict scale. The results show that there is a significant and positive spatial autocorrelation between LSTs, and urban landscape components are strong explainers of LST. A significant and positive effect of human daily activities on LST is captured at night, and this effect can last and accumulate over a few hours. The variables of land use functions and building forms show varying impacts on LST from daytime to nighttime. Moreover, the comparison between results at different scales indicates that the relationships between LST and some explainers are sensitive to the study scale. The current study enriches the literature on LST and offers meaningful and practical suggestions for the monitoring, early warning, and management of urban thermal environment with remote sensing technology and spatial big data sources.

Keywords: land surface temperature; MODIS; human daily activities; Weibo Check-in; spatial autoregressive model; spatial big data; Beijing



Citation: Wang, X.; Zhang, Y.; Yu, D. Exploring the Relationships between Land Surface Temperature and Its Influencing Factors Using Multisource Spatial Big Data: A Case Study in Beijing, China. *Remote Sens.* **2023**, *15*, 1783. <https://doi.org/10.3390/rs15071783>

Academic Editor: Hua Liu

Received: 16 February 2023

Revised: 18 March 2023

Accepted: 24 March 2023

Published: 27 March 2023



Copyright: © 2023 by the authors. Licensee MDPI, Basel, Switzerland. This article is an open access article distributed under the terms and conditions of the Creative Commons Attribution (CC BY) license (<https://creativecommons.org/licenses/by/4.0/>).

1. Introduction

In the past few years, more cities around the world have suffered the shock of extreme high temperature in summer [1–3]. Climate change is well-known as one of the main causes of global warming. In addition, the surface urban heat island (SUHI) effect further amplifies the influence intensity and trend of high temperature in cities. SUHI has been observed as a familiar phenomenon that the surface temperature in urban areas is higher than that in surrounding suburbs or rural areas [4–6]. SUHI exerts negative and harmful influences on the urban ecological environment and residents' health [7–11]. Things become worse when extreme heatwaves with a temperature higher than 36 °C last a long time in summer [12]. It leads to the decline of people's physical and mental abilities, and even death for some sensitive patients [12,13]. Therefore, it is of significance to investigate the variation pattern of UHI and its influencing factors for urban designers, planners, and policymakers. The findings could provide useful information and practical insights for urban healthy and sustainable development.

Land surface temperature (LST) is commonly used to measure the intensity of the SUHI effect [14–21]. Most previous studies focused on the effects of urban landscape factors on LST [15,22–24], such as the proportion of impervious surface and vegetation,

the configuration of buildings, and the urban layout. It is generally agreed that more vegetation or adding green infrastructure would lower the SUHI effectively [25–28]. Nevertheless, the cost of carrying out large-scale afforestation or building renewal on the already-existed urban landscape is usually enormous, especially in populous and facility-dense areas [21,29,30]. For this reason, it is necessary to propose and implement some more flexible and practical measures to alleviate the UHI effect.

On the other hand, studies also found that the intensity of human activities also casts strong, albeit fluctuating, influence on urban LST [31,32]. The impact of human activities on urban LST exists in both long-term and short-term. In the long run, human activities change the composition and configuration of the urban landscape dramatically. The impervious surface of buildings, roads, and other urban facilities increases radiation absorption and heat storage in urban areas, which is the leading cause of the SUHI effect [8,33,34]. From a short-term perspective, people's daily activities in cities rely heavily on the use of electrical appliances and vehicles. These activities are under less scrutiny for their effects on the UHI effects. In this study, we argue that if we can take effective measures to reduce the production of waste heat accompanied by people's daily activities, it will be beneficial to the strategies of urban heat mitigation. However, there is a lack of studies revealing how short-term human daily activities affect the LST in the daytime and nighttime. Moreover, there are two issues in existing studies that motivate the present study. On one hand, the heat does not stop conducting and fluxing at the boundary of data collecting units, and this leads to the spatial spillover effect of LST. This means that the LST of a certain area is not only affected by the determinants but also influenced by the LST of its surrounding areas [21,35,36]. However, traditional ordinary least square regression, which was widely employed in most of the previous studies, often does not take into consideration this spatial spillover effect [12–14,16,30,33,34,37]. This might result in misunderstanding and inefficiency to improve the urban thermal environment. On the other hand, pixels or grids are often used as the research unit due to the popularity of remote-sensing raster data [13,22,34,38,39]. Though they are fine scales to use to carry out studies, the practicality of their results is limited for administrative agencies. The basic unit for urban management and construction is the administrative unit, such as the community, street, or district. The difference between the scales of research affects the results and conclusions of LST studies, which is worthy of further investigation.

For these matters, the objectives of the present study were threefold: (1) We intended to construct a more integrated theoretical framework of LST by incorporating advanced remote-sensing-data-acquisition strategies through analyzing MODIS data, and the influence of human daily activities into the mechanism analysis. (2) We intended to depict LST patterns in daytime and nighttime and explore the impact of human daily activities on LST by employing spatial autoregressive models for both temporal periods. (3) We intended to analyze the similarities and differences of the results between the pixel scale and the administrative unit scale to provide practical urban-heat-island-effect-mitigation strategies. To this end, Beijing, one of the highly urbanized cities in China, is selected as a case city in this study. We collected MODIS remote-sensing products and Weibo check-in data to calculate LST and the intensity of residents' daily activities. We also collected LST influencing factors from multisource spatial big data, including point of interest (POI) data, building contour vector data, road network data, and 1km population and GDP grid data. We categorized the GIS vector data and gridded population and GDP data as spatial big data because of the spatial (1 km) and temporal (day and night) resolutions in the study. The remainder of this paper is organized in the sections below. Section 2 reviews the relevant works on the literature of LST, focusing on the diverse effects of its determinants. In Section 3, the data and methods of the current study are introduced. We also present the workflow of the study in this section. Following the results and analysis in Section 4, we discuss the implications, limitations, and future work in Section 4 and conclude the findings of the study in Section 6.

2. Literature Review

2.1. Urban Heat Island Effect and Land Surface Temperature

One of the most prominent features of urban climate is the urban heat island (UHI) effect. People discovered a long time ago that the thermal environment of urban areas is different from that of rural areas. In 1958, Manley [40] proposed the climatic term, “urban heat island”, for the first time to describe this abnormal phenomenon. With the rapid development of global urbanization, understanding UHI is attached to great importance in the urban design, construction, and management. In recent decades, heat waves usually enhance the intensity of UHI effect in megacities and raise widespread concerns about effective measures to attenuate the high temperature [6,41,42]. To some extent, the UHI effect in winter might be beneficial in energy saving, especially for some megacities in high-latitude countries [15,43]. However, rising temperature due to UHI effect leads to changes of local ecological environment and natural habitat for other species, which causes problems to urban livability. UHI not only brings pollutants to the air and water [44,45] and poses threats to urban biodiversity [46,47], but it also increases the health risks to urban residents [3,48] and raises environmental justice issues [17,49].

To understand the UHI effect, we must first measure this effect. Empirically, there are two types of indicators to quantitatively measure UHI effect: land surface temperature (LST) and air temperature [13,50–52]. While LST is not the same as near-surface air temperature, the two are closely related [53–55]. Air temperature is usually obtained from a fixed and limited number of meteorological stations, leading to a relatively weak ability to portray the temperature of continuous spatial sphere. LST is much more convenient to be collected across the a large area thanks to the rapid progress of remote-sensing technologies [19]. As a result, LST from multiple remote-sensing sources, such as Landsat TM satellite image [19,50,56,57], ASTER products [17], MODIS products [8,21,42,58], and others [59], has been widely adopted in recent studies.

Portraying the spatiotemporal patterns and trends of LST is one of the domains of LST studies [8,12,18,60]. On the one hand, LSTs show obvious differences across geographical locations regarding the background climates of research areas [50,61,62]. An LST study based on 32 major cities in China reveals that the annual mean urban–suburban temperature difference varies greatly from 0.01 °C to 1.87 °C in the daytime [33]. This spatial heterogeneity of LST is also verified in another study. Wang, Hessen, Samset, and Stordal [42] found that global LST is rising faster since 2001, though LST increase varies in different climatic regions. On the other hand, LSTs also show an obvious characteristic of temporal variation. The patterns of LST have been depicted and compared from different temporal perspectives, such as diurnal, seasonal, yearly, and even decadal change; large temporal fluctuations, especially seasonal fluctuations of LST, are also reported in many studies [14,18,42,57,58,61].

2.2. Influencing Factors of Land Surface Temperature

Another important topic of LST studies is to explore the influencing factors and their impacts on LST. The urban thermal environment is affected by a variety of factors, which can be summarized into four categories: urban landscape components, land-use functions, building forms, and socioeconomical conditions (especially daily human activities).

Urban landscapes include natural landscapes (forests, grassland, shrublands, wetlands, and water bodies) and artificial landscapes (roads, buildings, and other urban facilities). In the process of urbanization, natural landscapes have been converted dramatically into artificial landscapes [12,63]. Compared with vegetation and water, artificial landscapes, which are composed of cement, brick, asphalt, and metal, have a higher heat absorption rate and smaller specific heat capacity. Thus, the changes in land surface composition, especially the ratio of vegetation to impervious surface, modify the urban landscape and result in higher LSTs [22,41,64]. Expanding the area of vegetation and water bodies in the urban area has become a practical measure in urban high-temperature alleviation [29,63].

Different functions of urban land use also have varying impacts on the urban LST. Various land-use functions in a city provide specific urban facilities for human activities. Generally, business, office, and residence areas are characterized by skyscrapers, apartments, and townhomes, while green spaces are mainly composed of forests, grasslands, and lakes. This means that the capacities of diverse land-use functions in heat absorption and emission are different [58,64]. For example, Mohan et al. [65] assessed the UHI intensity of Delhi and observed the highest UHI in highly commercial areas. Wu, Yao, Zhuang, and Ren [37] revealed similar LST patterns in Beijing. Yao et al. [66] found that the impacts of commercial, industrial, recreational, and residential zones on UHI show obvious seasonal variations.

Urban landscape configuration also has a significant impact on urban LST. For our current study, however, since we focused only on a relatively small and densely populated area in Central Beijing, we represent urban landscape configuration with urban buildings because they are dominant in this current study area's urban landscape. In addition to the influence of building materials, urban high temperature can be partly attributed to building forms. The geometric properties of buildings, i.e., the height, width, area, and volume, are closely related to the absorption of solar radiation and the flux of air. Many studies have found that denser and taller buildings in a street tend to absorb and store more heat, and they are less likely to release heat into the air due to the urban canyon effect [19,25,36,64,67]. The influence of buildings on LST can also come from residents' activities or energy usage [10,53].

Socioeconomical conditions indicate the development level of a city, which is usually expressed in terms of population density and gross domestic product (GDP). Anthropogenic heat is the byproduct of socioeconomic development in a city. Some studies have found that a higher population density and higher GDP lead to a greater consumption of electricity and fossil energy, thus making them the main drivers of urban LST [13,21,30]. The effects of socioeconomical conditions on LST can be seen as the mediation of collective and long-term human activities. From a more macroscopic point of view, city sizes [4,6] and urban patterns [50] have also been shown to be important determinants of LST.

The conclusions of many previous studies provide positive strategies for mitigating high temperatures in cities, including urban greening, urban layout design, and land-use policies [29,50]. However, to date, few studies have explored the impact of short-term human daily activities on LST. As we previously argued, the transformation of urban landscape and land-use functions, the construction of buildings, and the development of urban economy take place in the progress of urbanization. Their effects on LST can be seen as the consequences of long-term human activities. On the contrary, human daily activities are diverse and instantaneous in urban areas. In this study, we refer to human daily activities as what urban residents experience and participate in during a 24-h period. They include home-based and work-based activities, commuting, shopping, dining out, and other leisure activities that happen in one day. Their changes in space and time are highly related to the use of electrical appliances and vehicles, resulting in complex LST patterns. The short-term effect of daily activities on LST performs at the hourly level and it is usually masked by the long-term activities. In the context of the rapid urbanization, it is important to explore and capture this short-term effect of daily activities for urban heat alleviation and energy management. This also provides a micromanagement strategy to mitigate the long-term urban heat island effect.

Based on these investigations, we summarize possible influencing factors of LST from different perspectives and present the mechanism diagram in Figure 1. Climatic factors (e.g., solar radiation, precipitation, and wind) and geographical factors (e.g., elevation, topography, and seaboard) might serve as the ultimate driving forces that define the spatiotemporal patterns of LST. These factors are less influenced by human activities, and their impacts are relatively stable over a long time. As for the influences of human activities, we can investigate them from a long-term perspective and a short-term perspective. The first three of the four categories of influencing factors mentioned above are essentially

the result of urbanization, which can be seen as the long-term human activities. Their effects on the LST change with the development of urbanization, such as urban sprawl and renewal. The influence of human daily activities on LST, by contrast, is short-lived due to fast-changing urban lifestyles. In the current study, we incorporated human daily activities into the analytical framework of LST in order to have a better understanding of the dynamics of LST in urban areas.

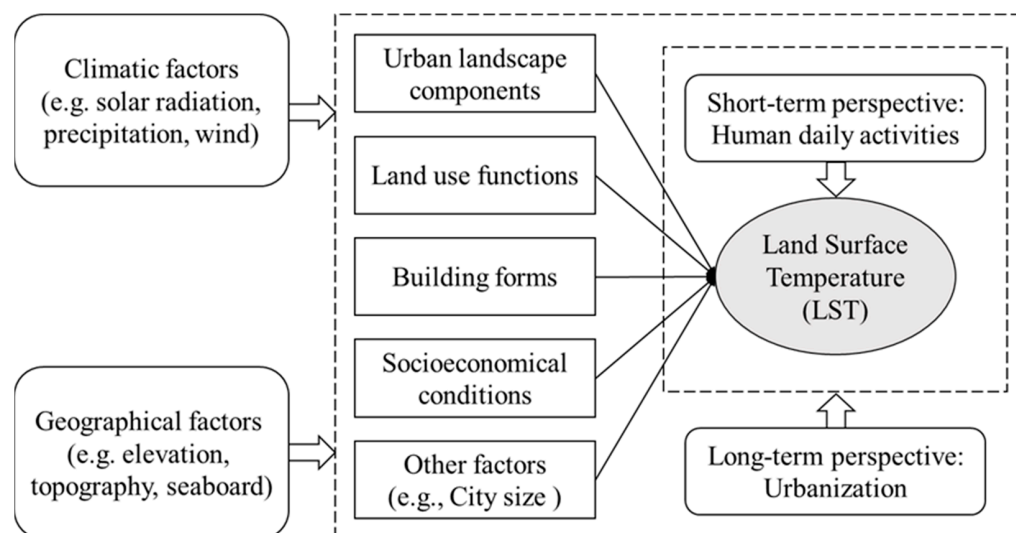


Figure 1. Possible influencing factors of LST from different perspectives.

3. Data and Methods

3.1. Study Area

Beijing is located in the north of the North China Plain (115°41'E–117°50'E, 39°44'N–41°05'N), with an area of 16,410 km². Beijing has a warm, temperate, semi-humid, and semi-arid monsoon climate. According to the data of the *Beijing Statistical Yearbook* in 2020, the average air temperature in Beijing is 13.8 °C. Beijing's annual extreme maximum temperature and minimum air temperature are 37.8 °C and −12.8 °C, respectively. Annual precipitation in Beijing is 527.1 mm, with a characteristic of main rainfall in the summer and autumn seasons. The resident population of Beijing in 2020 was 21.89 million, of which more than 19 million live in highly urbanized areas. The rapid urbanization since the 1980s leads to a quick sprawl of built-up area in Beijing, which increases from 1182 km² in 2004 to 1469 km² in 2019 (Figure 2). The impervious surfaces have replaced the vegetation and croplands in large areas, resulting in a severe UHI effect [26,37]. In 2019, the number of extreme high-temperature days in the whole year was 16 days, which was more than that in normal years (12.3 days). The central urban area of Beijing is the most populous and GDP-dense area; thus, it is an ideal case area for UHI and LST studies [22,23,25,66]. For the current study, we collected data for 135 subdistricts, namely street or town, in the central urban area of Beijing to investigate LST at the administrative unit level (Figure 2).

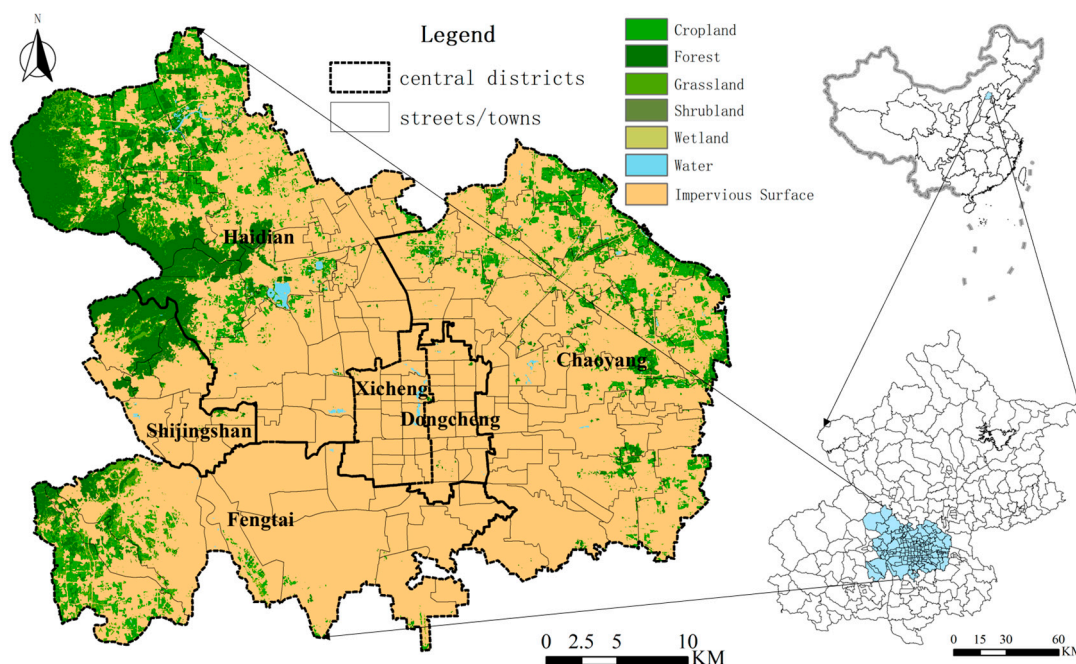


Figure 2. Study area: central urban area of Beijing, China.

3.2. MODIS Data for LST

Accurately measuring LST was one of the key tasks for the current study. As aforementioned, while air temperatures were traditionally used to measure the urban heat island effect and used in meteorological and climatic studies, LST has a better spatial and temporal consistency to represent the urban thermal landscape. In addition, LST and air temperature are closely related [31,68,69].

There are various remote-sensing images from multifarious satellites that can be used to extract LST data. In the present study, we adopted the Moderate Resolution Imaging Spectroradiometer (MODIS) product MOD11A1 (MODIS/Terra Land Surface Temperature/Emissivity Daily L3 Global 1 km SIN Grid) and MYD11A1 Version 6 datasets to calculate LST since, of the 36 spectral bands on board MODIS sensor, 20 spectral bands are used to measure brightness temperature in both infrared and visible parts of the electromagnetic spectrum. Although its spatial resolution is not as good as that of Landsat and other remote-sensing data, MODIS datasets provide “per-pixel Land Surface Temperature and Emissivity (LST&E) with a pixel size of 1000 meters (m). The product is produced daily in 5-minute temporal increments of satellite acquisition using the generalized split-window algorithm,” which makes the product an ideal source for LST data acquisition for our current study with minimal processing and comparably high accuracy [70]. This is because our study focuses on short-term human activities’ impact on LST. The impact of human daily activities on LST is assumed to be short-lived; hence, the high temporal resolution of the LST data was more important than spatial resolution in the current study.

MODIS datasets are available freely on the website <https://ladsweb.nascom.nasa.gov/search>, accessed on 8 February 2023 (under “Land/Land Surface Temperature & Emissivity” category), and a detailed introduction can be found at <https://lpdaac.usgs.gov/products/mod11a1v061/>, accessed on 8 February 2023. For land-surface-temperature extraction, the Two-Channel Algorithm radiative transfer model with bands 31 (thermal infrared band for brightness temperature measurement) and 32 (visible/near infrared band for reflectance) was used. After the Two-Channel Algorithm, advanced machine learning algorithms (including regression, kriging, and neural network algorithms) combined atmospheric profiles, surface types, zenith angle of the pixel view, observation time, and other ancillary data to fine-tune the LST and produce the final product that we used in our study. While the MODIS calculation of the LST considered multiple factors already, LST is affected more

so by natural and urban landscape factors in summer and winter [16,21]; the effect of human daily activities might not be as silent in these seasons. In order to investigate human activities' influence on urban LST, we chose the autumn season and selected MODIS images on 24 September 2014 for our daily investigation. During this season, the influence of human activities on LST is often more silent than during the summer/winter times, when the urban landscape and vegetation coverage might make human activities' influence on LST less detectable. For our study area, we used the MOD11A1 and MYD11A1 datasets to extract daytime LST (from 10:36 to 11:54 am) and nighttime LST (from 1:54 to 3:06 am), respectively. We chose these two time slots to extract the daytime and nighttime LST because these two periods are when the LST changes might be most influenced by the change of human activities. The daytime period is right after the city "wakes up." People commuted to work; offices were in full operation. The nighttime period is when the city "goes to sleep." Most people went to bed, and nighttime businesses closed. During these two periods, the changes of human activities' influence on LST are most silent. After spatial extraction and zonal computation, the LSTs of more than 1500 pixels and the 135 subdistricts are acquired and stored in a shapefile (administrative units) and a raster image (pixel level).

3.3. Spatial Big Data to Account for Human Activities

The measurement of human daily activities is another key source of data in this study. It used to be rather difficult, if not impossible, to capture the movement and aggregation of urban dwellers in the span of a day, or even if the data were recorded, they tended to be too chaotic and noise-burden for meaningful analysis. With the widespread use of smartphones, social media applications such as Twitter, Facebook, and Sina Weibo have emerged as enormous platforms for people to share their daily lives and activities. Advanced machine learning, meta-information extraction, and text-analysis algorithms are able to effectively organize and analyze these types of data now [71–75]. People's location information can be obtained easily after their authorization. These digital footprints are a good representative of human daily activities [76–78]. In this study, we collected the check-in data from Sina Weibo, the largest microblogging platform in China, to measure the number of active people at any given place and time (the data might be restricted for certain uses outside Mainland China; however, though similar data types, such as the geotagged Twitter data and Facebook posts that are widely available can be utilized for this type of research). Sina Weibo check-in data records the exact time, location (in geographic coordinates), and content of the Weibo (mini blog) when the user logged in. It is often regarded as a valuable resource for businesses and governmental organizations, for urban planning and design purposes. The location information was found to be reliable and is often used when referring to locational-based analyses [79–81]. As a matter of fact, during our preliminary exploration of the data, when the check-in data were overlaid with the road network map, a majority of them were on either side of the road, suggesting high locational accuracy for the current study. Even without content analysis, the location information of large numbers of users alone provides a strong indication of human gathering and spreading, an indication of the intensity of human activities. Moreover, the intensity of these active people is generally accompanied by heat emissions due to increased electrical appliance usage, concentrated vehicle usages, and even the mere gathering of large number of people, which play an important role in affecting urban LST in areas with heightened concentration. In our preliminary analysis, we created a spatial distribution (dot density map) of the check-in data, hoping to establish a visual link between the density of check-in and the variation of urban LST in the study area. The visual link, however, is less than ideal, partly because the daytime and nighttime urban LST do not vary greatly, partly because the check-in data are lumped together for the entire day (24 September 2014). To further investigate the daily pattern of how human behavior influences urban LST, we divided the check-in data of 24 September 2014, into 12 2-h slots to capture the temporal cumulative effect of human daily activities and how these accumulative activities impact urban LST.

We denoted the 2-h slots with the starting and ending time following a military clocking setting; for example, CI_1012 denotes the number of check-ins released from 10:00 am to 12:00 noon. Worth noting here is that human activities' impact on urban LST has a delayed effect [31,32]. To reflect this delayed effect, we use only the check-in data from 4:00 to 12:00 (CI46, CI68, CI810, and CI1012) as the influencing factors on urban daytime LST, while using the check-in data from 18:00 to 02:00 (CI1820, CI2022, CI2224, and CI2402) as the influencing factor on urban nighttime LST.

The land-cover map used in the present study was downloaded from the website <http://data.ess.tsinghua.edu.cn/>, accessed on 8 February 2023 [82]. It has a 10 m resolution and 11 level-1 land-cover types. Based on the thermal characteristics of the 11 level-1 land-cover types, we further summarize different land-cover types into 4 categories (i.e., vegetation, built-up land, water body, and other lands). After that, the proportion of each land-cover category, which was frequently used in previous studies [83–85], is calculated to represent the land-cover composition to control how land-cover types impact on urban LST. In addition, the normalized difference vegetation index (NDVI) is also obtained to portray vegetation coverage. The NDVI is derived from another MODIS product, MOD13Q1 (downloaded from <https://ladsweb.modaps.eosdis.nasa.gov/search>, accessed on 8 February 2023), following standard calculation with the near-infrared and red bands.

Point of interest (POI) was another data source used for this study. It belongs to emerging internet map data and contains the location information of various urban facilities and infrastructures. Due to its good explanatory power regarding land-use functions, it has been employed in many studies [76,80]. We collected 249,829 pieces of POIs in Beijing central districts from Baidu Map (maps.baidu.com; the POI data might be restricted for certain uses outside Mainland China. Similar POI data, such as the ones created from OpenStreetMap [86], is also used for detecting land function patterns). The raw POI data contain many different types. For the purpose of the current study, we followed previous practices [76,80,87] and grouped them into 3 categories based on their thermal characteristics to control the influence of land use functions on urban LST. These include consumption-related POI (CPOI), which includes POI of catering services, shopping service, recreation and entertainment; office-related POI (OPOI), which includes POI of corporate business, financial service, scientific research and education, medical and health, and government and administration; and vehicle-related POI (VPOI), which includes gas stations, car depot, and parking lots.

Building-form data are extracted from building-contour-vector data. A total of 487,687 pieces of building data in 2022 in the study area were downloaded from <https://data.yunshudu.com/index.html>, accessed on 18 December 2022. Through spatial overlay and calculation, we produced four indicators of building forms, e.g., average building area (Ave_Area), total building area (Sum_Area), average building volume (Ave_Volume), and total building volume (Sum_Volume), of each pixel and subdistrict to control the influence of urban construction on the urban LST.

Socioeconomical conditions at finer scales are difficult to obtain from traditional statistics. Fortunately, 1km grid population and GDP data (<http://www.resdc.cn>, accessed on 18 December 2022) in 2015 meet the requirement of indicator extraction at relatively flexible scales. The total resident population (Population), total GDP (GDP), and per capita GDP (PGDP) are computed at the pixel scale and subdistrict scale, respectively. Moreover, we extracted road network data from Open Street Map (OSM) in 2019 and calculated the length of road network (RoadLength) for each pixel and subdistrict. These datasets were used to control for the general socioeconomic background of the city on the urban LST. While we do realize that the data were not collected in the same year. We contend that the urban landscape's influence on urban LST remains relatively stable, since the central areas of Beijing were already highly developed, and changes of urban landscape over the years (2014–2020) might cause negligible changes regarding its influence on the urban LST.

3.4. Methods

Figure 3 illustrates the processing flow and methods used in the study; three methods are employed to analyze the patterns of LST and model the relationship between LST and its influencing factors: spatial autocorrelation analysis, Pearson correlation analysis, and spatial autoregressive model.

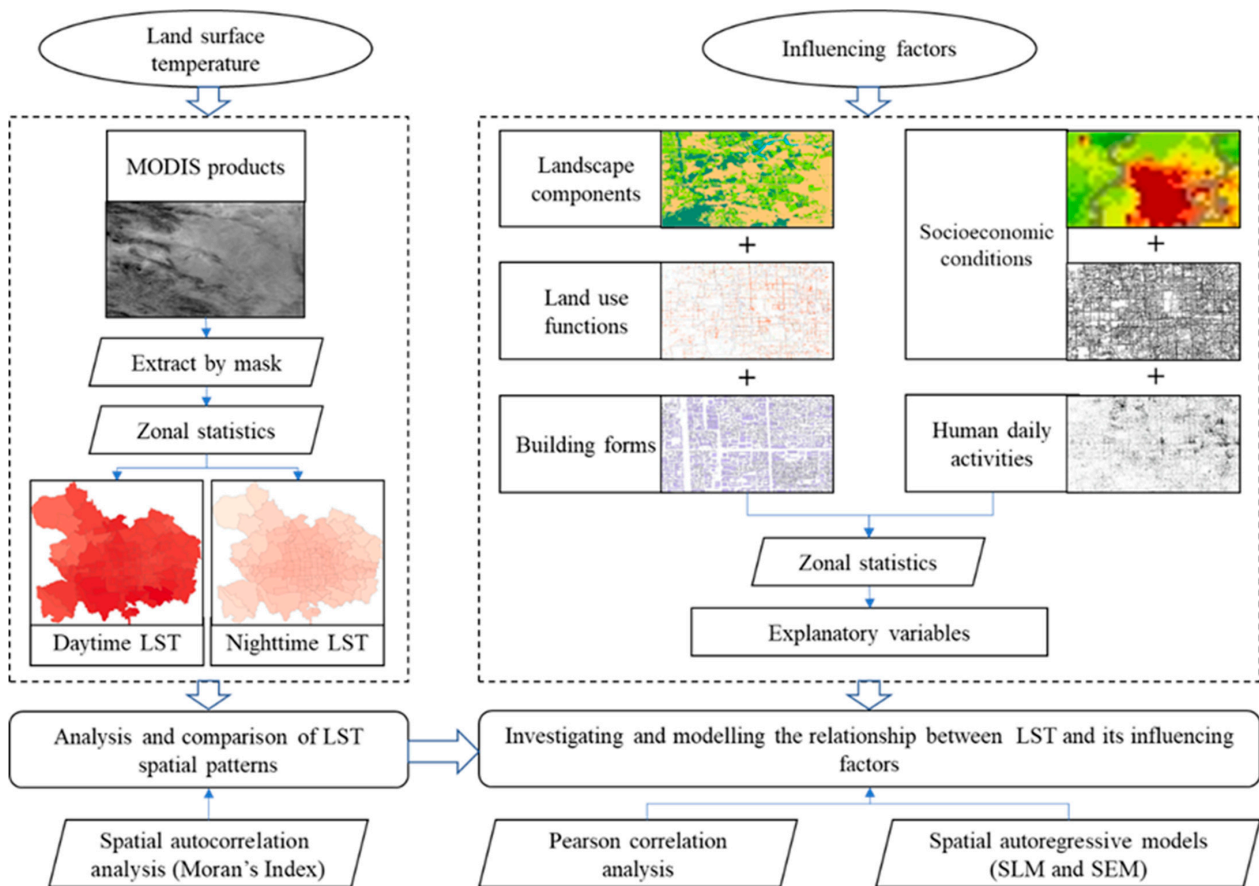


Figure 3. Processing flow and methods used in the study.

Spatial autocorrelation analysis: Considering the conduction and flux of heat in space, the LSTs between adjacent areas are highly related to one another. Moran's Index is widely adopted in studies [19,34,66] to test if the LSTs in different spatial locations are clustered, dispersed, or randomly distributed over the study area. Specifically, the global Moran's Index determines the existence and intensity of spatial autocorrelation overall, while the local Moran's Index is used to detect the location of significant clusters (local groups) or outliers (local anomaly). They are calculated as follows [88]:

$$I = \frac{n \sum_{i=1}^n \sum_{j \neq i}^n w_{ij} (x_i - \bar{x})(x_j - \bar{x})}{\sum_{i=1}^n (x_i - \bar{x})^2 \sum_{i=1}^n \sum_{j \neq i}^n w_{ij}} \quad (1)$$

$$I_i = \frac{(n-1)(x_i - \bar{x})}{\sum_{j \neq i}^n (x_j - \bar{x})} \sum_{j \neq i}^n w_{ij} (x_j - \bar{x}) \quad (2)$$

where x refers to the observed LST values, and w_{ij} is the spatial weight between two spatial units, i and j , in the spatial matrix W , which is an $n \times n$ matrix that defines the spatial neighborhood among spatial units. For detecting spatial autocorrelation, the binary weights (1 being neighbor, and 0 being non-neighbor) are often sufficient and are usually row-standardized for better interpretation and calculation [89]. By using the Moran's scatterplot

that is derived from the global Moran's Index formula [88], we can also distinguish four types of LSTs' local spatial associations: clusters of high values (high–high), clusters of low values (low–low), outliers with high value (high–low), and outliers with low value (low–high). More details of Moran's Index can be found in Anselin [89].

Pearson correlation analysis: To have an initial evaluation of each influencing factor's impact on the urban LST, and also to perform preliminary data exploration for the ensuing regression analysis, we conducted a pairwise Pearson correlation analysis to measure the linearity and strength of correlation between LST and its influencing factors. While the correlation analysis only analyzes the relationships between two variables without considering other influential factors, the results from correlation analysis provide an initial evaluation of the strength of relationships between the two variables in question; it has been a common practice in LST studies [16,25,66]. The values of Pearson correlation coefficient range from -1 to 1 , where a value closer to 1 (-1) indicates a stronger positive (negative) correlation, and 0 indicates no correlation between the LST and the identified factors.

Spatial autoregressive model: In the traditional ordinary least square (OLS) model, regression residuals are assumed to be independent. However, when a regression analysis was conducted using data collected over geographical spaces, the inherent spatial autocorrelation of geographical observations was highly likely to violate the assumption of residual independence [90]. It is likely to derive distorted or even wrong conclusions if we employ an OLS model to analyze spatial data [89,91]. In this study, we employed spatial autoregressive models to explore the impacts of influencing factors on LST due to potential spatial autocorrelation existing in the regular regression model's residuals. According to where the spatial autocorrelation of the residuals is believed to be from, two types of spatial autoregressive models, i.e., spatial lag model (SLM) and spatial error model (SEM), are often considered in empirical studies [63,89,92]. The former adds spatially autocorrelated dependent variable to the traditional ordinary least square (OLS) model, which believes the dependent variable's spatial autocorrelation is the primary cause for the residuals' spatial autocorrelation; and the latter takes into account the spatial autocorrelation of random errors, believing that the residuals' spatial autocorrelation is from the spatial autocorrelation of latent covariates. SLM and SEM can be expressed as follows:

$$\text{SLM} : y = \rho W y + \beta X + \mu \quad (3)$$

$$\text{SEM} : y = \beta X + \varepsilon, \varepsilon = \lambda W \varepsilon + \mu \quad (4)$$

where y and X refer to the explained variable and explanatory variables matrix (i.e., LST and its influencing factors in this study), respectively; ρ is the coefficient of $W y$, indicating the spatial lag of the dependent variable; λ is the coefficient of $W \varepsilon$, measuring the spatial autocorrelation of the latent covariates; and μ represents a well-behaved error term with a mean zero. Since often the sources of the residuals' spatial autocorrelation are usually weakly identifiable, in empirical studies, the Lagrange Multiplier (LM) or robust LM diagnostic tests are used for model selection [91]. In practice, the model that has a significant but smaller p -value of the (robust) LM statistics (less chance to make a type-I error) often is a more suitable alternative [89]. In addition, the Akaike Information Criterion (AIC) is used to compare the goodness-of-fit of models. The model with a smaller AIC is considered to be the better fit for the data [92].

4. Results

4.1. Spatiotemporal Patterns of LST

Table 1 shows the mean, minimum, maximum, range, standard deviation, and global Moran's Index of LST in the central area of Beijing. By analyzing the statistics, we can make several interesting observations. Firstly, the difference of LST in the daytime is always greater than that at night at both the pixel scale and subdistrict scale. The range of LST in the daytime is 1.33 °C and 0.54 °C, respectively, while, at nighttime, it falls to 0.71 °C

and 0.42 °C. These small ranges of land surface temperature within 24 h are expected during this time of the year. The results also suggest the LST information derived from the MODIS products is relatively stable and free from potential outliers' influence. Secondly, the LSTs at a larger scale tend to have a smaller variation. The standard deviation of LSTs at the subdistrict scale is 0.084 °C, both in the day and at night, which is smaller than that at the pixel scale, i.e., 0.152 °C and 0.120 °C. It can also be reflected by the comparison between the ranges at different scales. These two observations are expected from a physical thermal perspective for the most impervious urban surface. Energy fluctuation is more varied during daytime than nighttime, and the difference is more acute when measured at finer scale in cities. Thirdly, there is always a significantly positive spatial autocorrelation in LSTs, regardless of the pixel scale or the subdistrict scale. The values of the global Moran's Index range from 0.491 to 0.836, and they are all significant at the 99% confidence level. The spatial autocorrelation of LST can be attributed to heat flow in space [63]. If there is a difference in LST, heat conduction and flux from a high-LST area to surrounding low-LST areas will make the LSTs of adjacent areas tend to be the same, naturally causing the heightened global spatial autocorrelation pattern.

Table 1. Statistics of LST.

Scale	Time	Mean (°C)	Min (°C)	Max (°C)	Range (°C)	SD (°C)	Global Moran's Index
Pixel	Daytime	29.96	28.98	30.31	1.33	0.152	0.836 ***
	Nighttime	28.88	28.36	29.07	0.71	0.120	0.491 ***
Subdistrict	Daytime	29.99	29.62	30.16	0.54	0.084	0.669 ***
	Nighttime	28.96	28.63	29.05	0.42	0.084	0.817 ***

Note: *** indicates that the value is significant at 99% confidence level.

Another interesting finding from Table 1 is that the global Moran's Index at the pixel scale decreases at night, while the index at the subdistrict level at night is greater than that in the daytime. Combined with the distribution patterns of LST shown in Figures 4 and 5, we can have a better understanding of this interesting phenomenon. At the pixel scale, the clusters of similar LSTs are common in the central districts of Beijing in the daytime, except for the northwest of the Haidian District. During the nighttime, the decrease of LSTs in core urban area weakens the clusters of similar LSTs and leads to a smaller global Moran's Index. However, the data aggregation process makes the indexes at the subdistrict scale trend in the opposite direction. In the daytime, after averaging the pixels' LSTs to subdistricts, the number of similar LST clusters is reduced at the subdistrict scale, and it is reflected in a smaller global Moran's Index. When it turns to the night, data averaging eliminates the original difference of pixel-scale LSTs, making the spatial autocorrelation stronger at the subdistrict scale. Comparing Figure 4 with Figure 5, it is obvious that the distribution of subdistrict-scale LSTs at night shows a more agglomerated pattern than that at the pixel scale. This result also suggests that the Modifiable Areal Unit Problem that is common in geographic analysis needs to be treated carefully. Different conclusions might be drawn because of different scales of analysis. The result also justifies our investigation of the influencing factors of LST at these two scales and with human activities, which have distinctive day and night patterns.

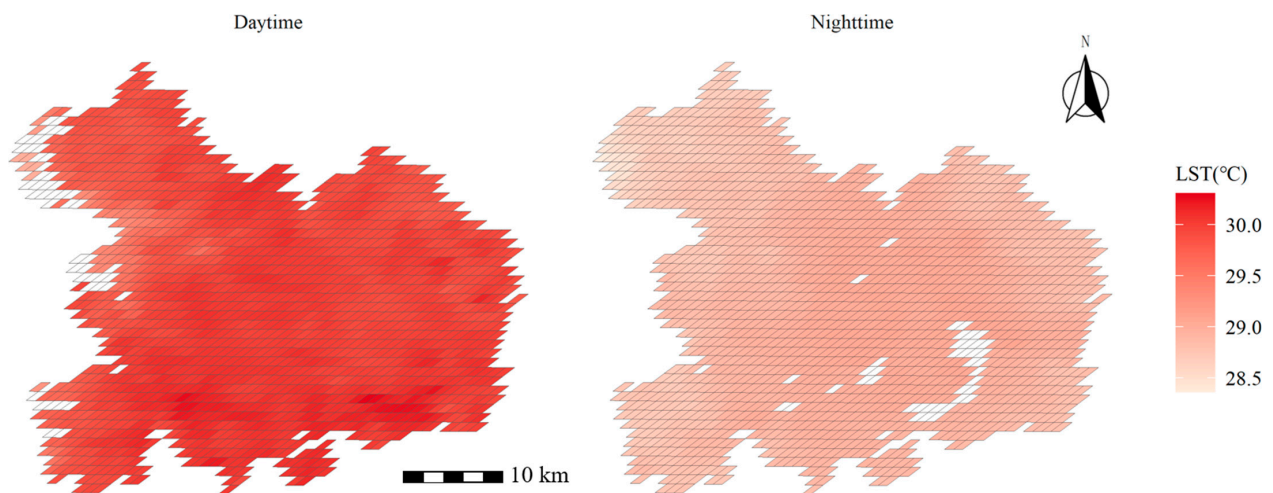


Figure 4. Distribution patterns of LST at pixel scale in central area of Beijing, China.

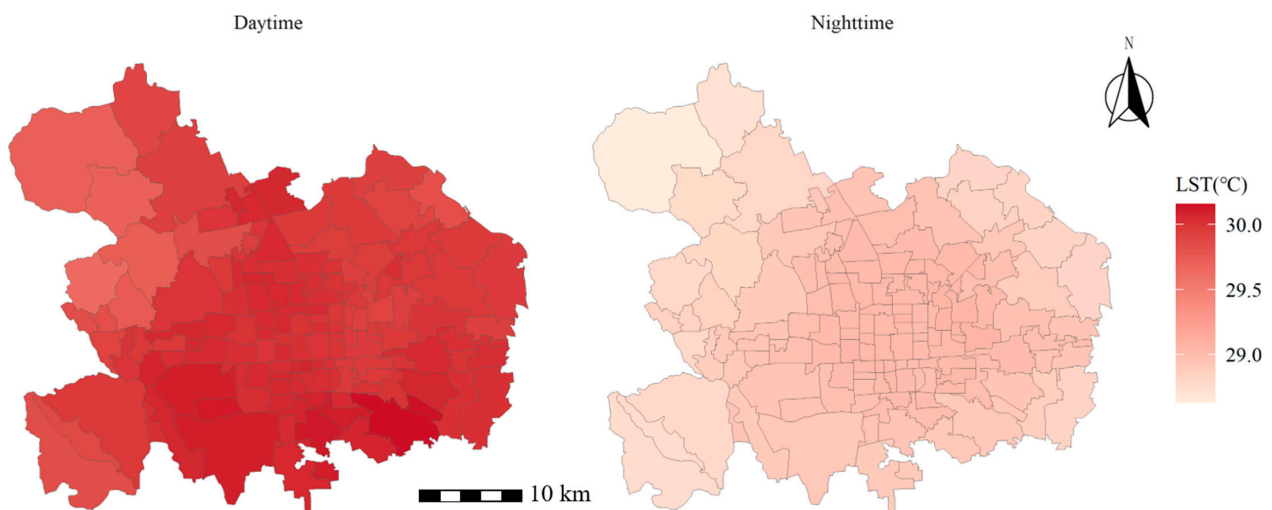


Figure 5. Distribution patterns of LST at subdistrict scale in central area of Beijing, China.

In order to reveal more details of LST's spatial autocorrelation, the results of the local Moran's Index at the pixel scale and subdistrict scale are mapped in Figures 6 and 7, respectively. Among the four types of local spatial autocorrelation, clusters of high LSTs (high–high) and clusters of low LSTs (low–low) are the dominant types in the central urban area of Beijing. Outliers with high LSTs (high–low) and outliers with low LSTs (low–high) are scattered only in a few areas in the daytime. These patterns are similar in both the pixel-level and district-level analysis. The LST distribution patterns vary from daytime to nighttime. In the daytime, high values of LST are mainly in the south areas, and low LSTs are distributed in the northwest area and several subdistricts in the northeast of Chaoyang District. At night, high LSTs are mainly in the central areas, and low LSTs mainly appear in the west and northeast areas. The distribution of LST shows a typical center–periphery pattern, and the temperature decreases from the center to the periphery. These patterns agree well with the human activities' distribution pattern in Beijing's central area during daytime and nighttime. The southern districts of the Central Beijing area are some of the busiest areas in Beijing during the daytime because many of the tourist sites and central governmental departments are located there. Traffic and people flows are high during the daytime, generating much energy that increases the urban LST. The central and northern parts of the Central Beijing area are where many of the nightlife facilities (bars, restaurants, and shopping malls) concentrate, which attracts many LST-increasing traffic and people flows during the nighttime. This exploratory spatial analysis is able to reveal a clear daily

LST shifting pattern that is related closely to the intensity of human activities, providing an empirical background for the ensuing influencing factors' investigation.

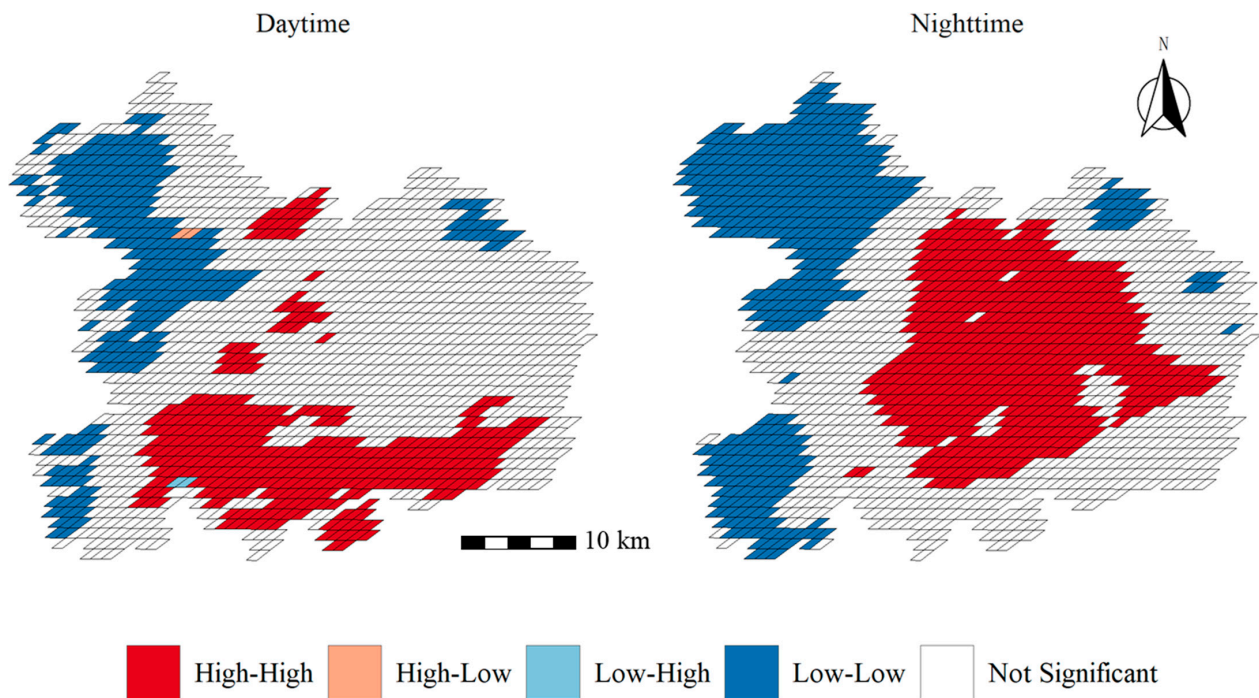


Figure 6. Local Moran's Index of LST at pixel scale in central area of Beijing, China.

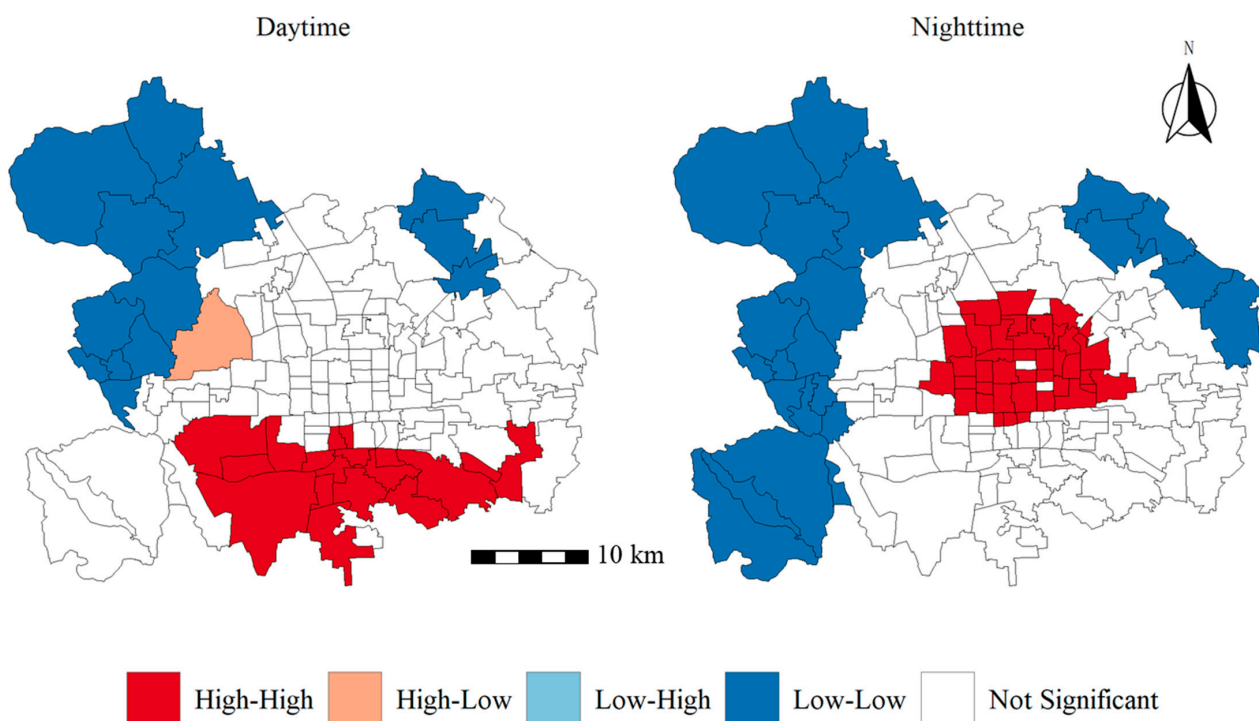


Figure 7. Local Moran's Index of LST at subdistrict scale in central area of Beijing, China.

4.2. Results of Pearson Correlation Analysis

By drawing scatter plots and conducting simple univariate regressions, we determined the relationships between the daytime LST and nighttime LST (shown in Figure 8). Although the local spatial cluster patterns of LSTs show a notable change from daytime to

nighttime (Figures 6 and 7), there is still a statistically positive correlation between them. At the pixel scale, 33% of the variation of nighttime LSTs can be explained by the daytime LST. When the daytime LST changes by 1 °C, it leads to an average LST change of 0.425 °C at night. The explanatory power of the daytime LST to the variation of the nighttime LST is weakened at the subdistrict scale ($R^2 = 0.27$), while the influencing factor between them becomes stronger ($\beta = 0.519$). This again suggests a modifiable areal unit problem (MAUP) problem. Coarser resolution at the subdistrict level aggregates the temperature variation, which causes a lower correlation between the daytime and nighttime temperatures and a bigger change for one degree of daytime temperature to nighttime temperature. The result further suggests that daily temperature changes are sensitive to scale effects, but more importantly, averaging land surface temperatures (LSTs) over longer periods could potentially mask subtle, but important influencing factors that have immediate effects, yet are often averaged; hence, they are ignored in long-term investigations, such as the daily human activities that fluctuate quickly over a day but smooth out in the long run. Our research intends to capture such factors' impact on urban LST for better planning purposes, more efficient urban management plans, better urban environments, and a more sustainable urban future.

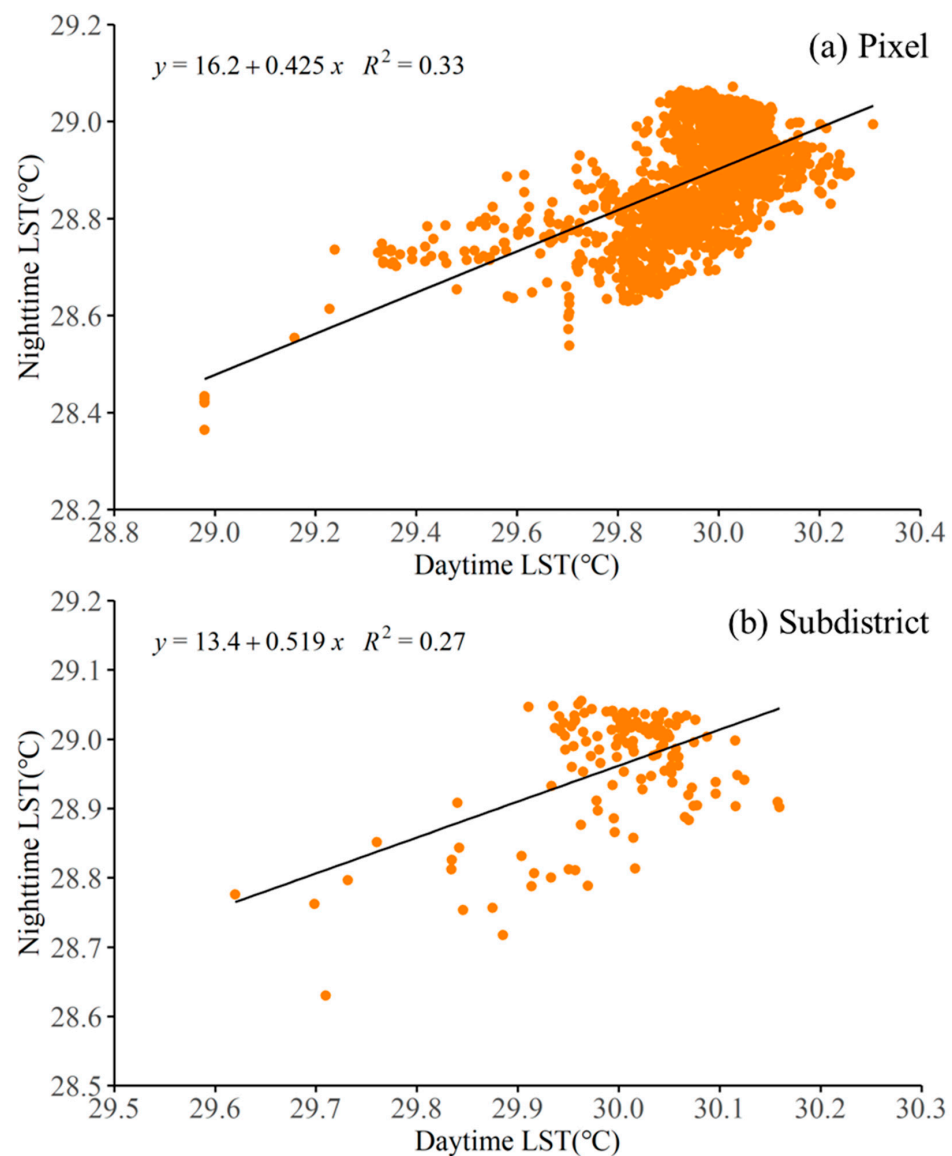


Figure 8. Relationships between the daytime LST and the nighttime LST.

According to the review in Section 2, we divide the LST’s influencing factors into five groups: (a) urban landscape components (NDVI, Vegetation, BuiltupLand, Water, and Others), (b) land-use functions (CPOI, OPOI, and VPOI), (c) building forms (Ave_Area, Sum_Area, Ave_Volume, and Sum_Volume), (d) socioeconomic conditions (Population, GDP, PGDP, and RoadLength), and (e) short-term human daily activities (CI_1012, CI_810, CI_68, and CI_46 in the day and CI_2402, CI_2224, CI_2022, and CI_1820 at night). The results of the Pearson correlation analysis between LST and these factors are plotted in Figures 9–18.

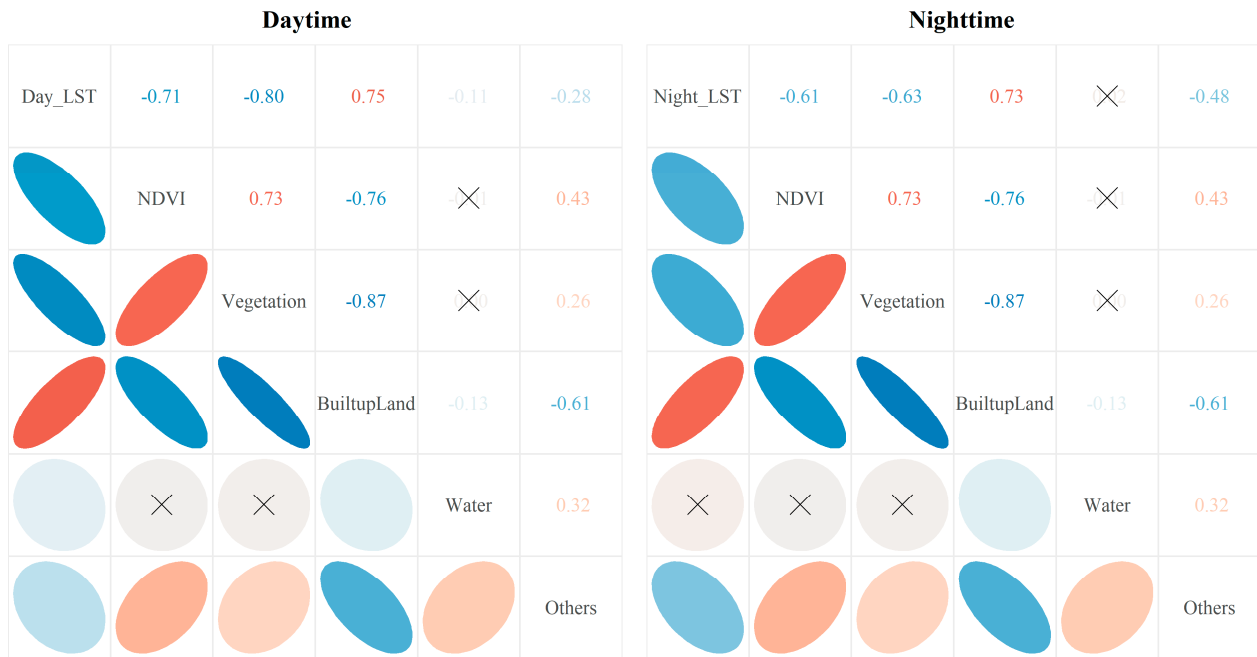


Figure 9. Pearson correlation coefficients between pixel-scale LST and urban landscape components. (Red series colors indicate positive correlations, and blue series colors indicate negative correlations. Flatter the shape, stronger the correlation. This applies to all correlation analysis figures.)

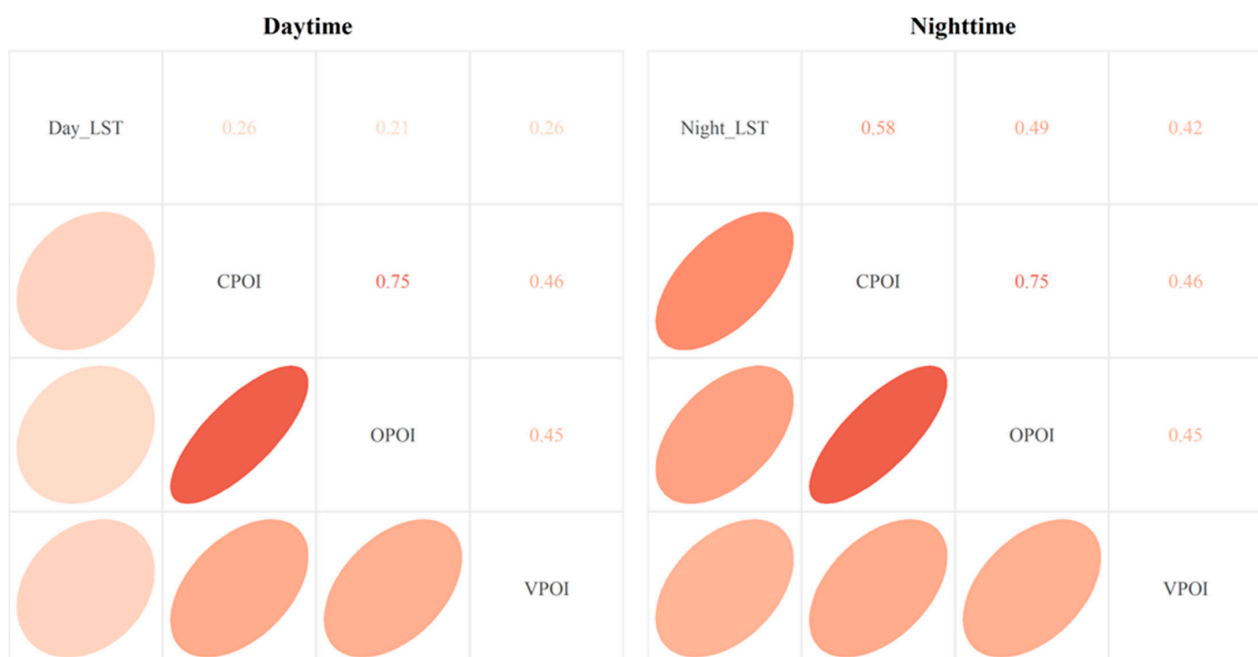


Figure 10. Pearson correlation coefficients between pixel-scale LST and land use functions.



Figure 11. Pearson correlation coefficients between pixel-scale LST and building forms.

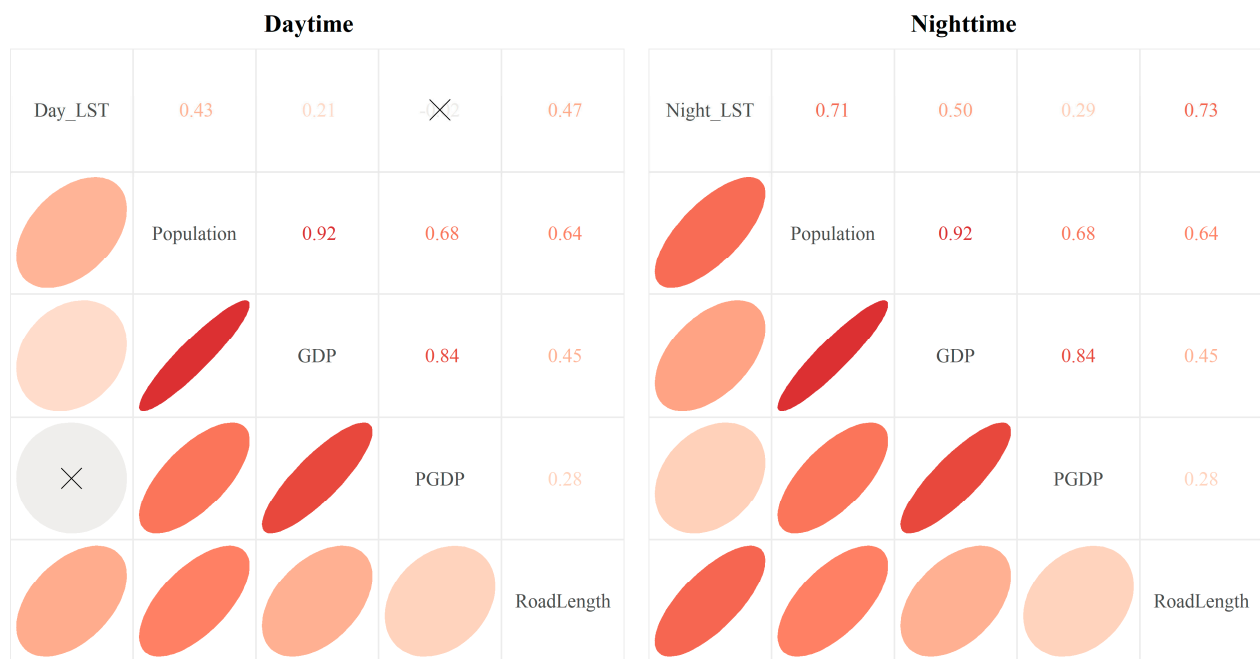


Figure 12. Pearson correlation coefficients between pixel-scale LST and socioeconomic conditions.

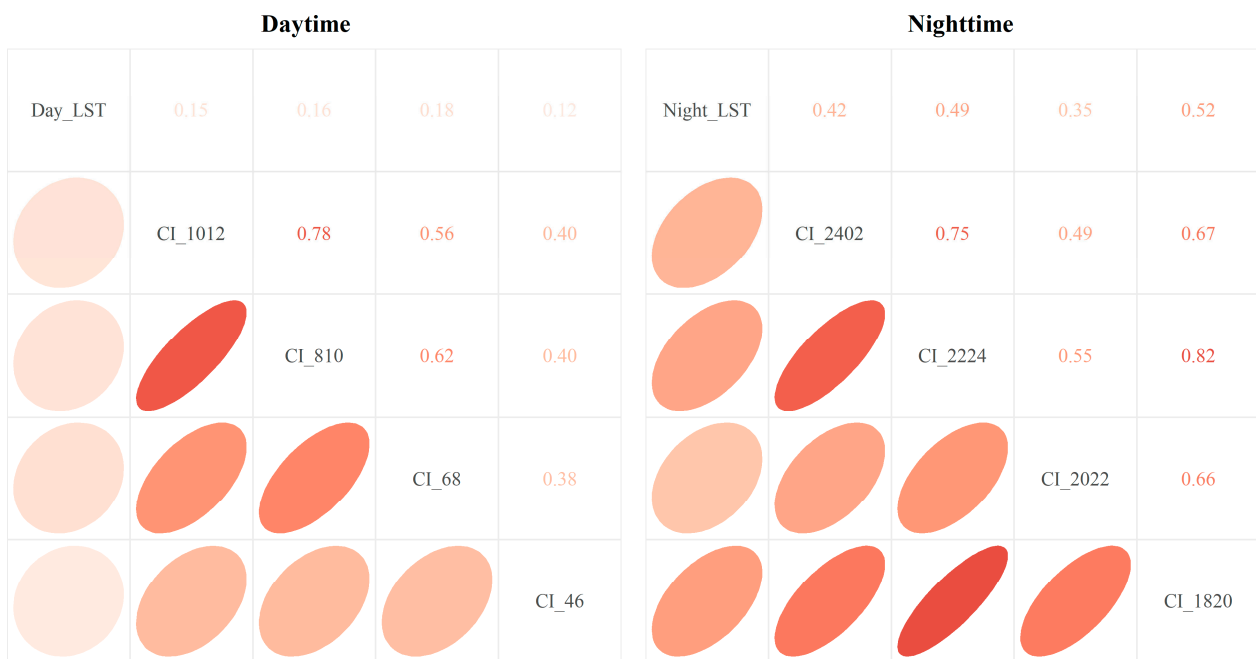


Figure 13. Pearson correlation coefficients between pixel-scale LST and short-term human daily activities.

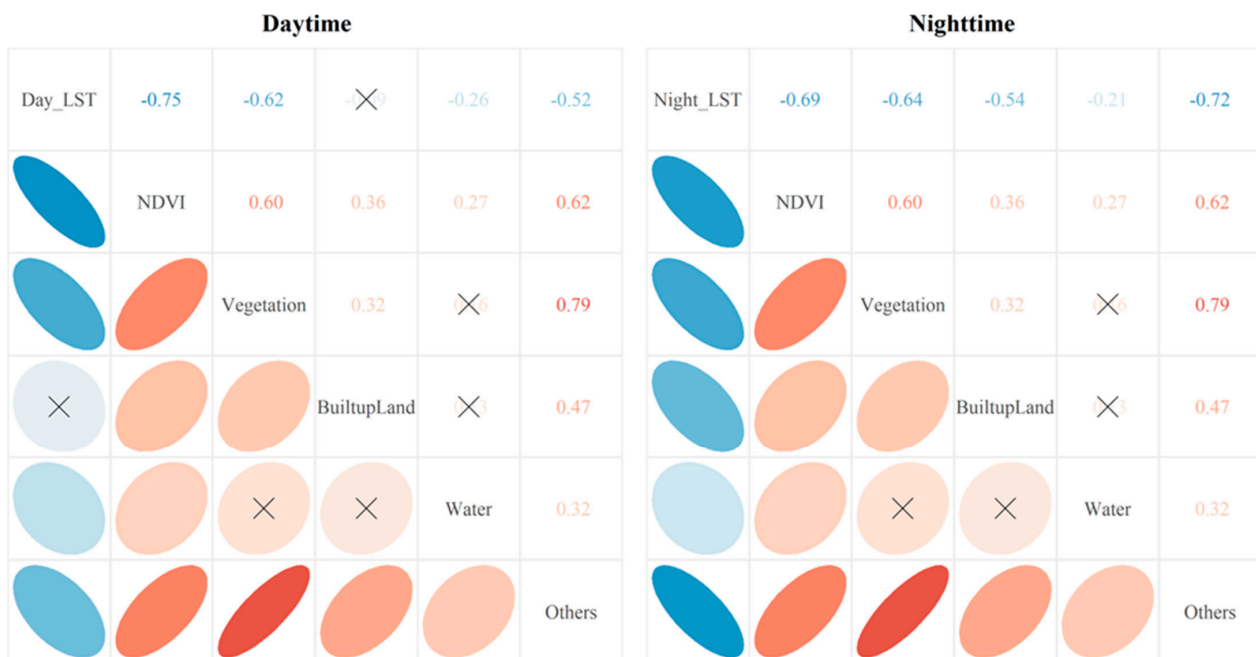


Figure 14. Pearson correlation coefficients between subdistrict-scale LST and urban landscape components.

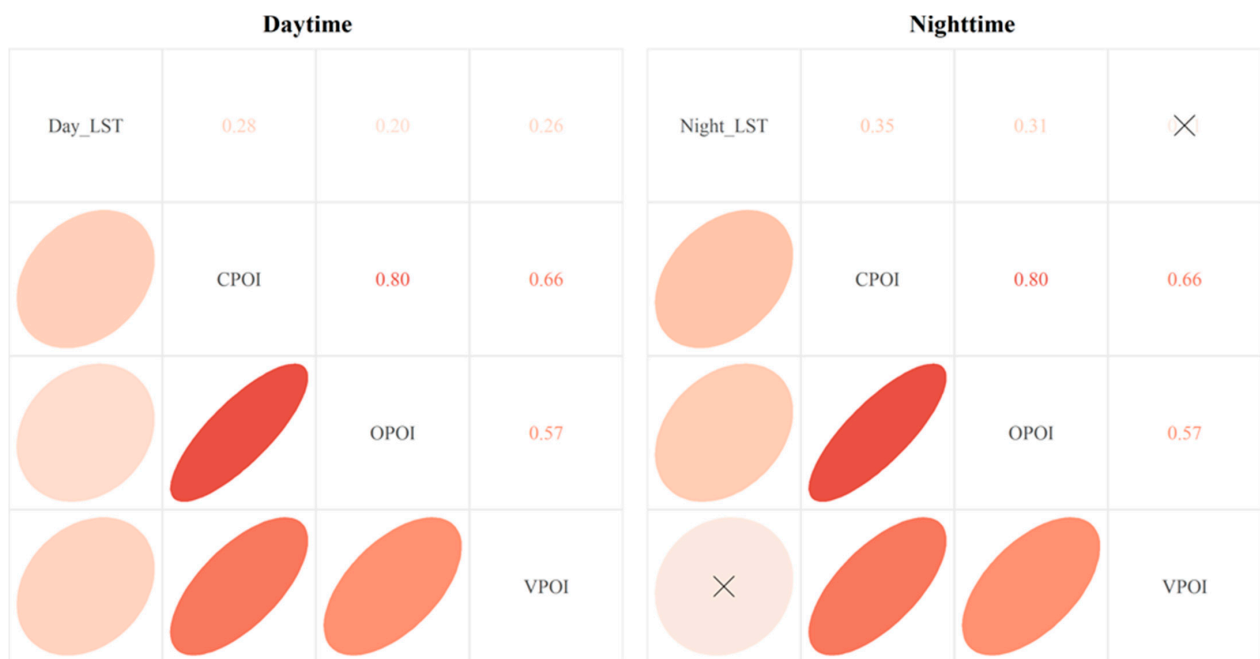


Figure 15. Pearson correlation coefficients between subdistrict-scale LST and land use functions.



Figure 16. Pearson correlation coefficients between subdistrict-scale LST and building forms.

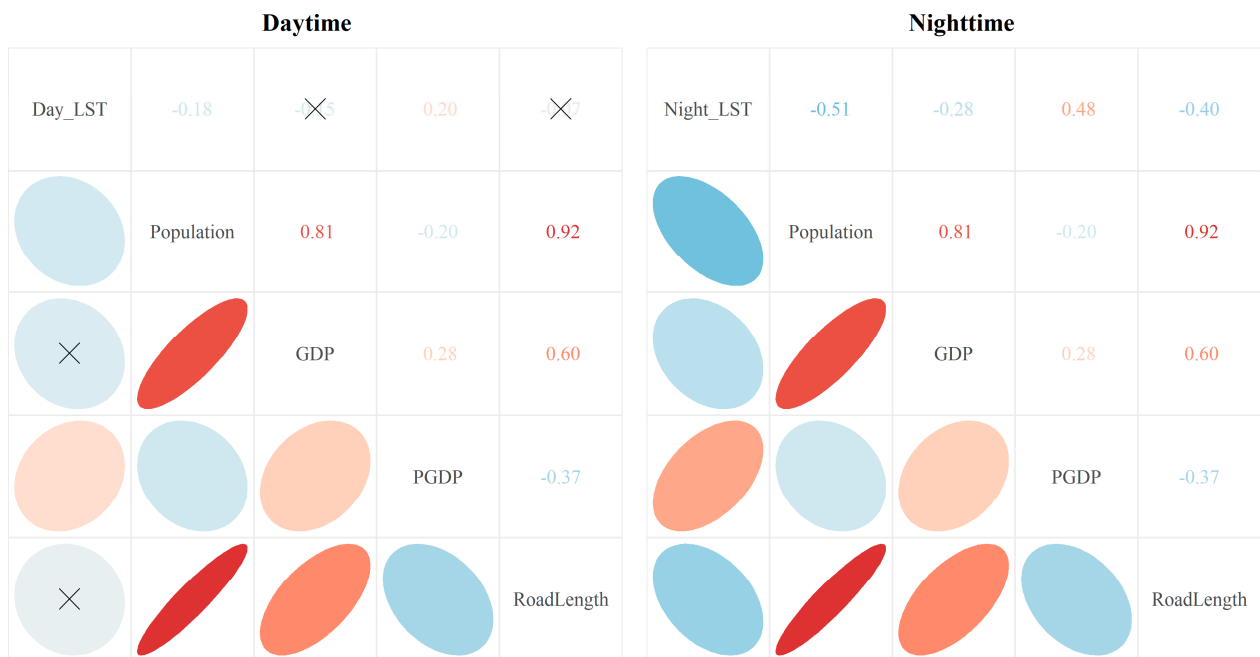


Figure 17. Pearson correlation coefficients between subdistrict-scale LST and socioeconomic conditions.

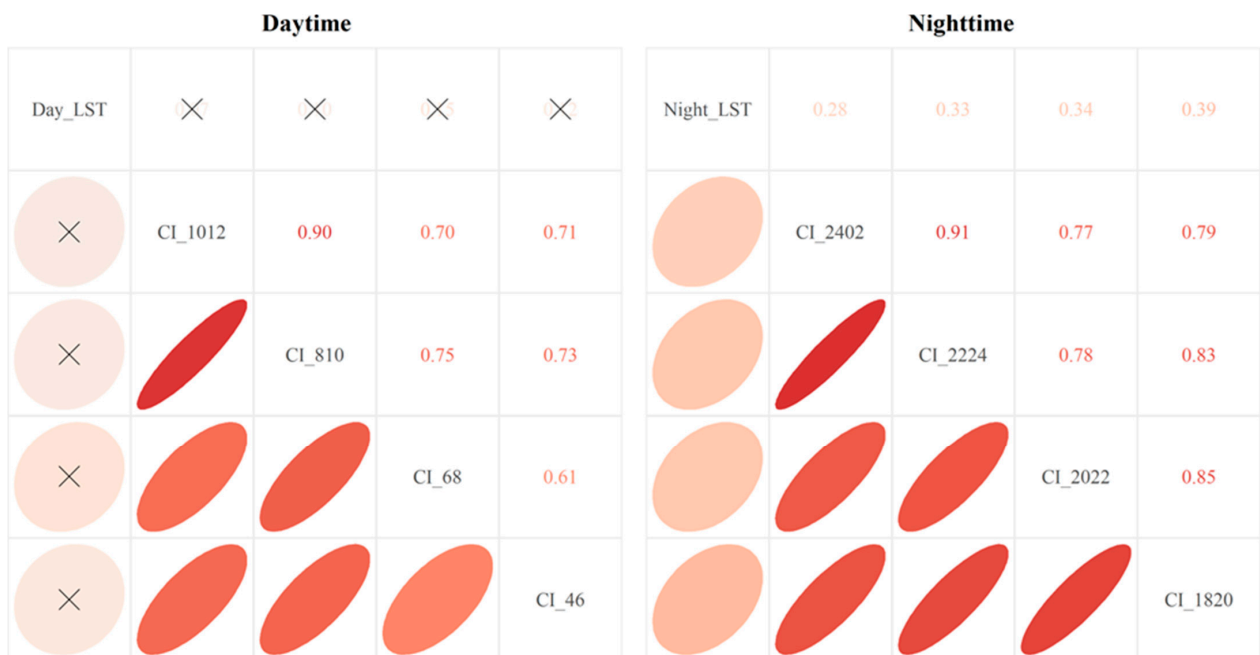


Figure 18. Pearson correlation coefficients between subdistrict-scale LST and short-term human daily activities.

At the pixel scale (Figures 9–13), significantly positive correlations between most influencing factors and the LST are found, except for several variables of urban landscape components. Among all the variables, the proportion of built-up land (BuiltupLand) has the largest positive coefficient (daytime, 0.75; and nighttime, 0.73), and the proportion of vegetation (Vegetation) shows the strongest negative correlation (daytime, −0.80; and nighttime, −0.63). The correlation coefficients of the variables in groups (b)–(e) are relatively small. This indicates that urban landscape components have a strong influence on urban LST, which is consistent with the conclusions of many previous studies [12,50,66]. By comparing daytime and nighttime coefficients, we find a general decrease in the absolute

values of coefficients in group (a). For instance, the absolute value of NDVI's coefficient decreases from 0.71 (daytime) to 0.61 (nighttime). On the contrary, the coefficients of all other variables in groups (b)–(e) show an obvious increase. For example, the coefficient of total building volume (Sum_Volume) increases from 0.41 in the day to 0.74 at night. These results signify that the impacts of urban landscape components on LST weakens at night while explanatory power of other variables become stronger. As for the variables of human daily activities, the correlation coefficients range from 0.12 to 0.18 in the daytime and 0.35 to 0.52 at night. This great increase suggests that, after solar radiation disappears at night, human activities become one of the crucial sources of heat production that increases urban LST. Moreover, there is also a significant correlation between the variables within each group. The correlation coefficient between NDVI and vegetation is 0.73 in group (a), and the population and GDP in group (d) have a strong correlation coefficient (0.92). Since NDVI and vegetation cover practically refer to the same thing, this is not surprising. The population and GDP are also strongly related in Central Beijing. These strong correlations suggest potential multicollinearity if all influencing factors are included without careful scrutiny.

At the subdistrict scale (Figures 14–18), some different findings emerge. In group (a), the proportion of built-up land (BuiltupLand) shows a nonsignificant correlation with LST in the daytime, while it turns to a significantly negative coefficient at night. In groups (b) and (c), the relationships between nighttime LST and vehicle-related POI (VPOI), total area of buildings (Sum_Area), average volume of buildings (Ave_Volume), and total volume of buildings (Sum_Volume) are statistically nonsignificant. In groups (d) and (e), GDP, road length, and all human daily activities are nonsignificant in the daytime. These correlations, which are different from that at the pixel scale, might be attributed to the following two reasons. The first possible explanation is that the relationship between LST and several explainers is sensitive to the research scale—a typical MAUP. In a specific region, a coarser scale aggregates and potentially masks relationships between LST and its influencing factors. This is also very important when analyzing influencing factors for urban LST since it has scale sensitivity. As a result, the above relationships become nonsignificant and even turn in the opposite direction. Another possible reason is that the thermal characteristics of some explainers vary at different scales and times. The specific heat capacity is an important property that determines the temperature variation of different materials. Due to a low specific heat capacity, impervious surface absorbs solar radiation fast in the daytime, leading to a quick rise in temperature. Meanwhile, after sunset, the temperature of impervious surface drops faster compared to water or vegetation [34]. This cooling effect of impervious surface at night might be vague and weak at the small scale, especially in the case of interference from other materials. With the expansion of the study scale, this effect is gradually revealed and shows a significant correlation with the LST at night. The nighttime positive coefficients of built-up land (BuiltupLand), average area of buildings (Ave_Area), and road length (RoadLength) might be partly attributed to the superposition of this scale effect and cooling effect.

4.3. Results of Empirical Regressions

Due to the possible multicollinearity problem, as we witnessed above, not all the explanatory variables that appear in the Pearson correlation analysis are used in the empirical models. As a matter of fact, since it is suspected that check-ins are potentially related with the size of population, we employ the stepwise regression method to filter explanatory variables until their variance inflation factors (VIFs) are less than 10. The tests suggest that while there is some type of correlation between check-ins and the size of the resident population, the VIF value of the two in the final regression model is less than 5; hence, they are both included in the final model. In addition, we also consulted previous theoretical studies [8,19,36] when choosing which particular variables to be included in the final model to avoid a data-driven study. The amount of impervious surface (road, and building area and volume) [93,94], vegetation coverage (NDVI) [95,96], and places that

attract many people and traffic flows (consumer and office places) [94] are often factors that are cited in studying urban land surface temperatures. After these initial primary analyses, our final model of the relationship between LST and its influencing factors can be expressed as follows:

$$\text{LST} = \beta_0 + \beta_1\text{NDVI} + \beta_2\ln\text{CPOI} + \beta_3\ln\text{OPOI} + \beta_4\ln\text{AveArea} + \beta_5\ln\text{AveVolume} + \beta_6\ln\text{Population} + \beta_7\ln\text{RoadLength} + \beta_8\ln\text{CI} \quad (5)$$

where LST refers to the values of LST, and CI denotes the number of check-ins. In this study, we build 12 models to investigate the impacts of human daily activities on LST at different scales and times. Models 1-6 use the pixel-scale data, while Models 7-12 use the subdistrict-scale data. In Models 1-3 and Models 7-9, the LSTs in the daytime are used as the outcome variables and other models use the nighttime LSTs. The check-ins in the daytime from 10:00 to 12:00 (CI_1012), from 8:00 to 12:00 (CI_0812), and from 06:00 to 12:00 (CI_0612); and the check-ins at night from 24:00 to 2:00 (CI_2402), from 22:00 to 2:00 (CI_2202), and from 20:00 to 2:00 (CI_2002) are used as explanatory variables to explore the potential cumulative effects of human daily activities. All explanatory variables are transformed by the natural logarithm, except NDVI, to eliminate the influence of their dimensions and to keep the function as linear as possible. The model is first estimated with ordinary least squares. As with all spatial data, the spatial autocorrelation of the ordinary least squares' residuals is tested via the Lagrange Multiplier test [97,98]. The test results clearly suggest that there is a significant spatial autocorrelation of the ordinary least squares model's residuals. To avoid misleading model results, spatial autoregressive models are more appropriate alternatives to the ordinary least squares model. As discussed in the methodology section, there are usually two forms of spatial autoregressive models, the spatial lag and spatial error model, depending on where the source of the spatial autocorrelation of the ordinary least squares model's residuals is. All the analyses and tests are conducted in the statistical software platform R [99] with the packages spdep [100] and spatialreg [101]. The analyses were performed on a PC laptop with Intel Core i5 8th CPU and 8 GB of memory.

In order to determine which spatial autoregressive model is more suitable, Lagrange Multiplier tests are again used, and the results are reported in Table 2. It is seen that RLMlag statistics are always greater and have lower p -values than RLMerr statistics, indicating that spatial lag model (SLM) tends to be a better choice. Therefore, Models 1–12 are estimated based on a SLM specification and their regression results are reported in Tables 3 and 4.

Table 2. Results of Lagrange Multiplier tests.

Scale	Time	RLMerr	p -Value	RLMlag	p -Value
Pixel	Daytime	9.4714	0.0021	113.07	$<2 \times 10^{-16}$
	Nighttime	8.6131	0.0033	139.64	$<2 \times 10^{-16}$
Subdistrict	Daytime	3.2102	0.0732	33.027	9.088×10^{-9}
	Nighttime	1.5385	0.2148	57.436	3.497×10^{-14}

Table 3. Results of SLM at pixel scale.

Variables	Model 1	Daytime Model 2	Model 3	Model 4	Nighttime Model 5	Model 6
(Intercept)	7.0452 *** (0.6710)	7.0034 *** (0.6690)	6.9712 *** (0.6679)	3.4061 *** (0.4422)	3.4828 *** (0.4439)	3.5009 *** (0.4452)
NDVI	−0.1833 *** (0.0228)	−0.1826 *** (0.0228)	−0.1823 *** (0.0228)	−0.00004 (0.0122)	−0.0006 (0.0120)	−0.0012 (−0.0120)
CPOI	−0.0005 (0.0021)	−0.0006 (0.0021)	−0.0006 (0.0021)	0.0029 *** (0.0011)	0.0024 ** (0.0011)	0.0023 ** (0.0011)
OPOI	0.0022 (0.0022)	0.0022 (0.0022)	0.0021 (0.0022)	0.0002 (0.0012)	−0.00008 (0.0012)	−0.0001 (−0.0012)
Ave_Area	0.0394 *** (0.0062)	0.0392 *** (0.0062)	0.0393 *** (0.0062)	−0.0042 (0.0031)	−0.0032 (0.0031)	−0.0032 (−0.0031)
Ave_Volume	−0.0285 *** (0.0039)	−0.0283 *** (0.0039)	−0.0283 *** (0.0039)	0.0028 (0.0019)	0.0021 (0.0019)	0.0021 (0.0019)
Population	0.0067 (0.0044)	0.0068 (0.0044)	0.0066 (0.0044)	0.0089 *** (0.0027)	0.0087 *** (0.0026)	0.0082 ** (0.0026)
RoadLength	0.0190 *** (0.0026)	0.0190 *** (0.0026)	0.0190 *** (0.0026)	0.0032 (0.0022)	0.0032 (0.0021)	0.0030 (0.0021)
CI_1012/2402	−0.0041 ** (0.0022)			0.0030 ** (0.0014)		
CI_0812/2202		−0.0032 (0.0021)			0.0045 *** (0.0011)	
CI_0612/2002			−0.0027 (0.0021)			0.0044 *** (0.0011)
w * LST	0.7605 *** (0.0226)	0.7618 *** (0.0225)	0.7629 *** (0.0224)	0.8779 *** (0.0157)	0.8753 *** (0.0157)	0.8749 *** (0.0157)
Model comparison						
AIC	−2291.3	−2290.2	−2289.5	−2770.9	−2781.9	−2782.2
AIC for lm	−1747.9	−1744.1	−1741.2	−1913.8	−1919.9	−1921.5

Note: *, **, and *** indicate significant at 0.1, 0.05, and 0.01 level, respectively.

Table 4. Results of SLM at subdistrict scale.

Variables	Model 7	Daytime Model 8	Model 9	Model 10	Nighttime Model 11	Model 12
(Intercept)	9.7291 *** (1.4727)	9.7386 *** (1.4776)	9.7444 *** (1.4830)	6.5270 *** (1.3862)	6.8181 *** (1.4308)	7.0980 *** (1.4579)
NDVI	−0.6753 *** (0.0686)	−0.6773 *** (0.0686)	−0.6783 *** (0.0686)	−0.1108 ** (0.0504)	−0.0885* (0.0492)	−0.0944 * (0.0488)
CPOI	−0.0167 ** (0.0077)	−0.0174 ** (0.0077)	−0.0177 ** (0.0077)	0.0103 (0.0065)	0.0094 (0.0065)	0.0088 (0.0064)
OPOI	0.0119 * (0.0063)	0.0118 * (0.0063)	0.0115 * (0.0063)	−0.010 * (0.0052)	−0.0089 * (0.0052)	−0.0096 * (0.0052)
Ave_Area	0.0427 ** (0.0180)	0.0433 ** (0.0180)	0.0434 ** (0.0181)	−0.0222 (0.0153)	−0.0258 * (0.0152)	−0.0275 * (0.0151)
Ave_Volume	−0.0389 *** (0.0111)	−0.0396 *** (0.0111)	−0.0397 *** (0.0111)	0.0238 ** (0.0093)	0.0249 *** (0.0092)	0.0260 ** (0.0091)
Population	−0.0168 *** (0.0062)	−0.0165 *** (0.0062)	−0.0164 *** (0.0062)	−0.0046 (0.0054)	−0.0060 (0.0052)	−0.0059 (0.0052)
RoadLength	0.0299 *** (0.0094)	0.0299 ** (0.0094)	0.0300 *** (0.0094)	−0.0124 (0.0083)	−0.0112 (0.0081)	−0.0106 (0.0080)
CI_1012/2402	−0.0032 (0.0036)			0.0134 *** (0.0034)		
CI_0812/2202		−0.0023 (0.0038)			0.0146 *** (0.0034)	
CI_0612/2002			−0.0015 (0.0041)			0.0159 *** (0.0034)
w * LST	0.6836 *** (0.0487)	0.6834 *** (0.0488)	0.6832 *** (0.0490)	0.7794 *** (0.0469)	0.7688 *** (0.0484)	0.7588 *** (0.0494)
Model comparison						
AIC	−512.11	−511.69	−511.47	−554.40	−556.64	−559.75
AIC for lm	−413.65	−413.64	−414.01	−454.83	−460.29	−465.55

Note: *, **, and *** indicate significant at 0.1, 0.05, and 0.01 level, respectively.

After analyzing the results presented in the tables above, we extracted several meaningful findings that we would like to share. First, SLM performs better than traditional OLS

estimation, and the LST has a significant spatial spillover effect. By comparing the AICs in the last two rows of Tables 3 and 4, we can see that all AICs for spatial models (-2782.2 to -2291.3 at pixel scale and -559.75 to -512.11 at subdistrict scale) are much smaller than the AICs for nonspatial models (-1921.5 to -1747.9 at pixel scale and -465.55 to -413.65 at subdistrict scale). According to the criteria proposed by Anselin [89], smaller AICs indicate that SLM fit the data better for all models. The coefficients of spatially lagged dependent variable ($w*LST$) range from 0.6832 to 0.8779 and are always statistically significant at the 0.01 level. Not surprisingly, this suggests that the LST in a specific region is heavily influenced by the LST of adjacent regions. However, the spatial spillover effect of LST was often ignored in previous global empirical studies [12–14,16,17,21,30,33,34,37]. This study validates the better applicability of the spatial model than conventional nonspatial models in LST studies. Additionally, this finding can also provide inspiration for relevant policy making. The inefficiency of a cooling measure in a specific region is likely to be the result of the influence of surrounding high temperature. Hence, it is necessary to take global and systematic measures to improve urban thermal environment and mitigate high temperatures.

Second, a significantly positive effect of human daily activities on LST is captured at night, and this effect may accumulate over a few hours. All coefficients of check-ins (CIs) are statistically nonsignificant in the daytime, except for one coefficient at the pixel scale. In contrast, all nighttime coefficients of check-ins (CIs) are significantly positive at the 0.01 level. This finding is consistent with the research of Peng, Jia, Liu, Li, and Wu [16]; and Jia and Zhao [21]. Both research teams found that the influences of explainers on LST vary with the change of temperature from daytime to nighttime. The difference of the effect of human daily activities between daytime and nighttime is possibly caused by two reasons: the global difference between daytime LST and nighttime LST and the change of main heat source after sunset. During the daytime, the impact of human daily activities on urban LST is comparably weak, which is easily eclipsed by other strong explainers, such as NDVI, reflectance of the impervious surface, and concrete rooftops. After sunset, human-related heat emissions from traffic, catering, and electric appliances become determinant heat sources for LST. Therefore, the contribution of human daily activities to LST is stronger and more statistically significant at night. The values of coefficients indicate that when the number of check-ins increase by 1% , the nighttime LST increases by 0.0030 °C to 0.0159 °C. Additionally, we find that the coefficient of CI_2402, which is collected from 24:00 to 2:00, is the smallest among three different time slots. CI_2202 (0.0045) and CI_2002 (0.0159) show the strongest impacts on LST at pixel scale and subdistrict scale, respectively. This suggests that the LST at a specific time is likely to be affected not only by the human activities occurred at that time but also by the lagged and cumulative influence of human activities within a few hours. Check-ins are often posted by consumers before dinner to share their lives or get discounts from the restaurants. Meanwhile, their influence on temperature mainly relies on the process of consumption.

Third, the modeled results also suggest that the impacts of various LST explainers exhibit notable variations between daytime and nighttime. NDVI exerts a negative effect on LST, but at the pixel level, NDVI is nonsignificant during nighttime. Qiao et al. [102] suggest that this abnormal relationship might be due to the absence of plant transpiration at nighttime, reducing vegetation cover's cooling effects. The coefficients of consumption-related POI (CPOI) are negative in the day, and they turn to positive at night, which is opposite in variation to office-related POI (OPOI). In fact, since there is practically no material difference among various land-use functions, the difference of their effects on urban LST essentially comes from the residents' daily activities at different times. During the daytime, offices are the main places where people work and socialize. After work, people usually go to restaurants, shopping malls, and bars, leading to a surge in anthropogenic heat emissions in those places. Similarly, the coefficients of average area (Ave_Area) and average volume (Ave_Volume) of buildings change reversely from daytime to nighttime. A building with a larger area means a faster absorption and dissipation of heat, and larger-volume buildings

usually have higher heights. Solar radiation during the daytime is obstructed by high-rise buildings, resulting in a shadow effect. Meanwhile, at night, high-rise buildings block the heat dispersion in the vertical direction [62]. Population shows a significant and positive effect on LST at pixel level during night, while its impact on LST at the subdistrict level is significantly negative during the daytime. These results are consistent with previous studies, such as in [8,13]. These studies, however, do not provide in-depth discussions on why such phenomena were observed. From our investigation in the field and consultation with local meteorologists, we contend that since the distances between workplaces and residence places in Beijing are generally far, population data derived from statistic grid data might not indicate true human activities during the daytime. These population data might reflect more about the information of residence places. Therefore, its negative impact on daytime LST is unexpected at the larger scale. As for the effect of road length (RoadLength) on LST, it is significantly positive during the daytime but turns to nonsignificant at night. This can be ascribed to the small specific heat capacity of cement and the intensity of traffic during the daytime but reduced at night.

Fourth, the various factors' impact on urban LST has a strong MAUP, in that different effects (even opposite effects) are observed at the pixel and subdistrict levels. For instance, from Tables 3 and 4, it is observed that the absolute values of the coefficients of CI in Models 4–6 are smaller than those in Models 10–12. Check-ins are relatively sparse at the pixel level, so its effect is weak. By summing them up to a larger scale, collective human activities can produce a scale effect, turning it into a strong explanatory variable. The variation of resolution or scale might lead to different effects of one variable, and this scale sensitivity has been investigated and discussed in relevant studies [50,63]. Our study adds new evidence to this interesting and meaningful finding. It is important to recognize this finding for policy making. Human activities' influence on urban LST is particularly scale-sensitive since the influence of human activities is a collective influence. Only when there is a higher concentration of a larger number of human beings will the human activities' influence on urban LST show significant effects, both statistically and practically. This finding, while unsurprising, was seldom discussed in previous studies; however, it poses an important indication for sustainable urban planning and management. Our modeled results with two different scales suggest that to reduce the potential urban heat island effect in megacities such as Beijing or other large cities in China and beyond, urban planners need to strategically allocate and build up a variety of different land-use functions within the limited space; interweave impervious surfaces with parks, green spaces, and waterbodies; avoid too densely distributed monotonic building types; and balance between convenience, accessibility, and anthropogenic heat production.

5. Discussion

5.1. Implications for Urban Sustainable Development

The current study contributes to the studies of everyday urbanism [103,104]. The results of the current study add to the knowledge and provide detailed strategies for urban planners and managers to build a greener and more sustainable city. First, the significant spatial autocorrelation of LST shows that LST is affected by both the local factors and the factors of surrounding areas. The thermal environment of surrounding regions is an important factor when carrying out cooling measures to alleviate high temperatures in hot spot regions during heat waves. The implementation and effect evaluation of heat-alleviation measures also need to be strategically designed based on appropriate scales. This means that the cooling measures to alleviate high temperatures should be coordinated from a global rather than a local perspective. For example, the cooling effect of a single and small vegetation is very limited, while the warming effect of the expansion of an impervious surface is relatively great. A reasonable spatial layout of built-up lands, vegetations, and water bodies in cities is necessary for mitigating SUHI.

Second, social-media big data become an increasingly important source to depict and understand human activities, including the intensity, trend, and other hard-to-acquire

characteristics from traditional sources. Our study demonstrates that it can be applied to produce strategies to micromanage urban land surface temperature. Although a significant impact of human daily activities on LST during the daytime is not present from our model, likely because of the prevalence of urban land configuration's influence, human activities at nighttime projects impact on urban land surface temperature. Using social media data, we have the capacity to predict the changes of land surface temperature particularly after sundown. When we combine traditional meteorological data, remote-sensing data, and social-media big data, the management of urban micro meteorological conditions will be more timely, accurate, and efficient.

Third, human daily activities have a significant positive influence on LST at night. After sunset, the heat generated by human activities becomes one of the main sources of urban LST. The accompanying energy-consumption activities, such as gasoline, natural gas, and electricity, can be easily captured by social-media big data. This will facilitate the management of energy supply and consumption. The flexibility of energy and electricity supply can also be improved according to the tides and trends of human activities after sunset, thus providing strategies to alleviate energy-supply pressure and reducing unnecessary energy consumption.

5.2. Limitation and Future Work

This study proposes a new idea for LST studies: to explore the impact of human daily activities on LST from a short-term perspective. While we are able to produce evidence that short-term human daily activities have a positive influence on urban land surface at night, we are not able to establish a relationship during the daytime primarily because urban LST is strongly related to urban land configurations (large amount of impervious surface) during the daytime. Landscape configuration factors, such as the density and index of patch, edge, and shape, are significant explainers of LST [17,20,105], but they are not included in the current study. It will be one of our concerns to take landscape configuration factors into LST studies in future work. In addition, this study uses data from only one day in autumn to establish the linkage between short-term human activities and urban LST. While our initial consideration is to avoid the extreme summer or winter weather to mask human activities' influences on urban LST, it might merit further investigations using different days in different seasons, such as summer and winter, to see whether the conclusions presented in the current study still hold. Moreover, the mechanism of the impact of different variables on urban LST is complex; it is highly likely that different intensities of human activities in different places might project different influences on urban LST. This means that the influence degree of LST's factors may vary greatly across the study area, especially at different scales. The model presented in the current study (spatial autoregressive model) assumes the influence is the same at all pixels/subdistrict, and while this might hold true for smaller areas as in the current study, it might not be tenable when we investigate a city with a more complex land-cover composition and more varied land-use categories. Therefore, further investigation into the spatial heterogeneity of mechanism will be needed.

6. Conclusions

In this study, we specifically investigated human daily activities' influence on urban LST and re-examined the relationship between LST and its influencing factors at a two-hour interval basis on one autumn day. Our study yields several important and novel findings for future LST studies and guidance for sustainable urban planning and management. First, check-in data serve as a good proxy for human daily activities [79,81,86,106,107]. In some previous studies [13,19,33], grid population data or nighttime light data are used to represent the activities of urban residents. However, these data are static and make it difficult to capture people's real-time dynamics or short-term activities that are often masked out during long-term studies. Check-ins released by users can be easily obtained at any time. The flexibility and timeliness of check-in data coincide with the

characteristics of human daily activities better than gridded estimation. Second, the spatial patterns of LST in Central Beijing varies from daytime to nighttime. In the daytime, the high clusters of LST are mainly distributed in the south, while the nighttime LST shows a typical characteristic of the center–periphery decline pattern. There is a high correlation between daytime LST and nighttime LST, though. Third, from a short-term perspective, human daily activities have been found to affect LST significantly after sunset, and its impacts may last and accumulate over a few hours. Along with human daily activities, waste heat produced by traffic and electric appliances increases rapidly. During the daytime, urban landscape components are strong explainers of LST because of their thermal properties; hence, the effect of human activities is veiled. Meanwhile, at night, anthropogenic activities and induced heat emissions become the main provider of heat, leading to an increase of LST. For urban managers, the use of check-in data can bring new ideas to the monitoring and early warning for extreme heat. The flexibility of energy and electricity supply can also be improved according to the tides and trends of human daily activities, thus alleviating energy-supply pressure and reducing unnecessary energy consumption that might contribute to an elevated land-surface temperature. Fourth, scale sensitivity and the cumulative effect are recommended to be taken into consideration when modeling LST and its influencing factors and making UHI mitigation policies. The results from this study suggest that the impacts of influencing factors on LST at the pixel scale and subdistrict scale are different. The thermal environment of surrounding regions is an important factor when carrying out cooling measures to alleviate high temperature in hot-spot regions. The implementation and effect evaluation of heat-alleviation measures also need to be strategically designed based on appropriate scales.

Urbanization in China has been undergoing a rapid development in recent decades. High-temperature management is commonly concerned in the construction of a livable, healthy, and sustainable city [8,20,61]. As one of the most urbanized cities in China, Beijing’s experience in urban construction and management is often learned and referenced by other cities. The current study highlights the impact of short-term human daily activities on LST and provides insightful and practical conclusions for dealing with a high urban temperature. We expect the study to enrich other LST studies and bring about a better understanding of LST management for sustainable urban development in the future.

Author Contributions: Conceptualization, X.W., Y.Z. and D.Y.; methodology, X.W., Y.Z. and D.Y.; software, X.W. and D.Y.; validation, X.W., Y.Z. and D.Y.; formal analysis, X.W. and D.Y.; investigation: X.W. and D.Y.; resources, X.W., Y.Z. and D.Y.; data curation, X.W.; writing—original draft preparation: X.W.; writing—review and editing: X.W., Y.Z. and D.Y.; visualization: X.W.; supervision, Y.Z. and D.Y. All authors have read and agreed to the published version of the manuscript.

Funding: This research was funded by the Scientific Research Foundation for the Introduced Talents of Putian University, China, grant number (2023010); and Social Science Foundation of Fujian Province, China, grant number (FJ2023MGCA037).

Data Availability Statement: The datasets used in the article are available from the mentioned websites or the corresponding author upon reasonable request.

Acknowledgments: The authors are thankful for the helpful comments and suggestions provided by the reviewers and editors.

Conflicts of Interest: The authors declare no conflict of interest.

References

1. Shah, P.B.; Patel, C.R. Integration of Remote Sensing and Big Data to Study Spatial Distribution of Urban Heat Island for Cities with Different Terrain. *Int. J. Eng.* **2023**, *36*, 71–77. [[CrossRef](#)]
2. Oroud, I.M. Integration of GIS and remote sensing to derive spatially continuous thermal comfort and degree days across the populated areas in Jordan. *Int. J. Biometeorol.* **2022**, *66*, 2273–2285. [[CrossRef](#)] [[PubMed](#)]
3. Heaviside, C. Urban Heat Islands and Their Associated Impacts on Health. In *Oxford Research Encyclopedia of Environmental Science*; Oxford University Press: Oxford, UK, 2020.
4. Oke, T.R. City size and the urban heat island. *Atmos. Environ.* **1973**, *7*, 769–779. [[CrossRef](#)]

5. Oke, T.R. The Heat Island of the Urban Boundary Layer: Characteristics, Causes and Effects. In *Wind Climate in Cities*; Cermak, J.E., Davenport, A.G., Plate, E.J., Viegas, D.X., Eds.; Springer: Dordrecht, The Netherlands, 1995; pp. 81–107.
6. Zhou, B.; Rybski, D.; Kropp, J.P. The role of city size and urban form in the surface urban heat island. *Sci. Rep.* **2017**, *7*, 4791. [[CrossRef](#)]
7. Maimaitiyiming, M.; Ghulam, A.; Tiyip, T.; Pla, F.; Latorre-Carmona, P.; Halik, U.; Sawut, M.; Caetano, M. Effects of green space spatial pattern on land surface temperature: Implications for sustainable urban planning and climate change adaptation. *Isprs J. Photogramm. Remote Sens.* **2014**, *89*, 59–66. [[CrossRef](#)]
8. Rao, Y.X.; Dai, J.Y.; Dai, D.Y.; He, Q.S. Effect of urban growth pattern on land surface temperature in China: A multi-scale landscape analysis of 338 cities. *Land Use Policy* **2021**, *103*, 105314. [[CrossRef](#)]
9. Heaviside, C.; Macintyre, H.; Vardoulakis, S. The Urban Heat Island: Implications for Health in a Changing Environment. *Curr. Environ. Health Rep.* **2017**, *4*, 296–305. [[CrossRef](#)] [[PubMed](#)]
10. Li, X.; Zhou, Y.; Yu, S.; Jia, G.; Li, H.; Li, W. Urban heat island impacts on building energy consumption: A review of approaches and findings. *Energy* **2019**, *174*, 407–419. [[CrossRef](#)]
11. Simwanda, M.; Murayama, Y. Spatiotemporal patterns of urban land use change in the rapidly growing city of Lusaka, Zambia: Implications for sustainable urban development. *Sustain. Cities Soc.* **2018**, *39*, 262–274. [[CrossRef](#)]
12. Heintl, M.; Hammerle, A.; Tappeiner, U.; Leitinger, G. Determinants of urban-rural land surface temperature differences—A landscape scale perspective. *Landscape Urban Plan.* **2015**, *134*, 33–42. [[CrossRef](#)]
13. Siddiqui, P.; Tariq, M.; Ng, A.W.M. An Investigation to Identify the Effectiveness of Socioeconomic, Demographic, and Buildings' Characteristics on Surface Urban Heat Island Patterns. *Sustainability* **2022**, *14*, 2777. [[CrossRef](#)]
14. Chen, X.; Zhang, Y.P. Impacts of urban surface characteristics on spatiotemporal pattern of land surface temperature in Kunming of China. *Sustain. Cities Soc.* **2017**, *32*, 87–99. [[CrossRef](#)]
15. Zhang, Y.; Sun, L.X. Spatial-temporal impacts of urban land use land cover on land surface temperature: Case studies of two Canadian urban areas. *Int. J. Appl. Earth Obs. Geoinf.* **2019**, *75*, 171–181. [[CrossRef](#)]
16. Peng, J.; Jia, J.L.; Liu, Y.X.; Li, H.L.; Wu, J.S. Seasonal contrast of the dominant factors for spatial distribution of land surface temperature in urban areas. *Remote Sens. Environ.* **2018**, *215*, 255–267. [[CrossRef](#)]
17. Connors, J.P.; Galletti, C.S.; Chow, W.T.L. Landscape configuration and urban heat island effects: Assessing the relationship between landscape characteristics and land surface temperature in Phoenix, Arizona. *Landscape Ecol.* **2013**, *28*, 271–283. [[CrossRef](#)]
18. Luintel, N.; Ma, W.; Ma, Y.; Wang, B.; Subba, S. Spatial and temporal variation of daytime and nighttime MODIS land surface temperature across Nepal. *Atmos. Ocean. Sci. Lett.* **2019**, *12*, 305–312. [[CrossRef](#)]
19. Yang, L.Q.; Yu, K.Y.; Ai, J.W.; Liu, Y.F.; Yang, W.F.; Liu, J. Dominant Factors and Spatial Heterogeneity of Land Surface Temperatures in Urban Areas: A Case Study in Fuzhou, China. *Remote Sens.* **2022**, *14*, 1266. [[CrossRef](#)]
20. Zhang, Q.; Wu, Z.X.; Singh, V.P.; Liu, C.L. Impacts of Spatial Configuration of Land Surface Features on Land Surface Temperature across Urban Agglomerations, China. *Remote Sens.* **2021**, *13*, 4008. [[CrossRef](#)]
21. Jia, W.X.; Zhao, S.Q. Trends and drivers of land surface temperature along the urban-rural gradients in the largest urban agglomeration of China. *Sci. Total Environ.* **2020**, *711*, 134579. [[CrossRef](#)]
22. Huang, C.D.; Ye, X.Y. Spatial Modeling of Urban Vegetation and Land Surface Temperature: A Case Study of Beijing. *Sustainability* **2015**, *7*, 9478–9504. [[CrossRef](#)]
23. Xiao, R.-B.; Ouyang, Z.-Y.; Zheng, H.; Li, W.-F.; Schienke, E.W.; Wang, X.-K. Spatial pattern of impervious surfaces and their impacts on land surface temperature in Beijing, China. *J. Environ. Sci.* **2007**, *19*, 250–256. [[CrossRef](#)]
24. Yang, J.; Sun, J.; Ge, Q.S.; Li, X.M. Assessing the impacts of urbanization-associated green space on urban land surface temperature: A case study of Dalian, China. *Urban For. Urban Green.* **2017**, *22*, 1–10. [[CrossRef](#)]
25. Zhang, N.Y.; Zhang, J.J.; Chen, W.; Su, J.J. Block-based variations in the impact of characteristics of urban functional zones on the urban heat island effect: A case study of Beijing. *Sustain. Cities Soc.* **2022**, *76*, 103529. [[CrossRef](#)]
26. Yao, L.; Sun, S.; Song, C.; Li, J.; Xu, W.; Xu, Y. Understanding the spatiotemporal pattern of the urban heat island footprint in the context of urbanization, a case study in Beijing, China. *Appl. Geogr.* **2021**, *133*, 102496. [[CrossRef](#)]
27. Chen, Y.; Shen, L.Y.; Zhang, Y.; Li, H.; Ren, Y.T. Sustainability based perspective on the utilization efficiency of urban infrastructure—A China study. *Habitat Int.* **2019**, *93*, 17. [[CrossRef](#)]
28. Lyu, R.F.; Zhang, J.M.; Xu, M.Q.; Li, J.J. Impacts of urbanization on ecosystem services and their temporal relations: A case study in Northern Ningxia, China. *Land Use Policy* **2018**, *77*, 163–173. [[CrossRef](#)]
29. Meerow, S.; Keith, L. Planning for Extreme Heat. *J. Am. Plan. Assoc.* **2022**, *88*, 319–334. [[CrossRef](#)]
30. Bokaie, M.; Zarkesh, M.K.; Arasteh, P.D.; Hosseini, A. Assessment of Urban Heat Island based on the relationship between land surface temperature and Land Use/Land Cover in Tehran. *Sustain. Cities Soc.* **2016**, *23*, 94–104. [[CrossRef](#)]
31. Huang, H.C.; Yang, H.L.; Deng, X.; Hao, C.; Liu, Z.F.; Liu, W.; Zeng, P. Analyzing the Influencing Factors of Urban Thermal Field Intensity Using Big-Data-Based GIS. *Sustain. Cities Soc.* **2020**, *55*, 102024. [[CrossRef](#)]
32. Xie, M.; Zhu, K.G.; Wang, T.J.; Feng, W.; Gao, D.; Li, M.M.; Li, S.; Zhuang, B.L.; Han, Y.; Chen, P.L.; et al. Changes in regional meteorology induced by anthropogenic heat and their impacts on air quality in South China. *Atmos. Chem. Phys.* **2016**, *16*, 15011–15031. [[CrossRef](#)]
33. Zhou, D.C.; Zhao, S.Q.; Liu, S.G.; Zhang, L.X.; Zhu, C. Surface urban heat island in China's 32 major cities: Spatial patterns and drivers. *Remote Sens. Environ.* **2014**, *152*, 51–61. [[CrossRef](#)]

34. Wang, C.Y.; Li, Y.B.; Myint, S.W.; Zhao, Q.S.; Wentz, E.A. Impacts of spatial clustering of urban land cover on land surface temperature across Koppen climate zones in the contiguous United States. *Landsc. Urban Plan.* **2019**, *192*, 103668. [[CrossRef](#)]
35. Tran, D.X.; Pla, F.; Latorre-Carmona, P.; Myint, S.W.; Gaetano, M.; Kieu, H.V. Characterizing the relationship between land use land cover change and land surface temperature. *ISPRS J. Photogramm. Remote Sens.* **2017**, *124*, 119–132. [[CrossRef](#)]
36. Guo, A.D.; Yang, J.; Xiao, X.M.; Xia, J.H.; Jin, C.; Li, X.M. Influences of urban spatial form on urban heat island effects at the community level in China. *Sustain. Cities Soc.* **2020**, *53*, 101972. [[CrossRef](#)]
37. Wu, Z.F.; Yao, L.; Zhuang, M.Z.; Ren, Y. Detecting factors controlling spatial patterns in urban land surface temperatures: A case study of Beijing. *Sustain. Cities Soc.* **2020**, *63*, 102454. [[CrossRef](#)]
38. Wang, S.M.; Ma, Q.F.; Ding, H.Y.; Liang, H.W. Detection of urban expansion and land surface temperature change using multi-temporal landsat images. *Resour. Conserv. Recycl.* **2018**, *128*, 526–534. [[CrossRef](#)]
39. Guo, G.H.; Wu, Z.F.; Xiao, R.B.; Chen, Y.B.; Liu, X.N.; Zhang, X.S. Impacts of urban biophysical composition on land surface temperature in urban heat island clusters. *Landsc. Urban Plan.* **2015**, *135*, 1–10. [[CrossRef](#)]
40. Manley, G. On the frequency of snowfall in metropolitan England. *Q. J. R. Meteorol. Soc.* **1958**, *84*, 70–72. [[CrossRef](#)]
41. Morabito, M.; Crisci, A.; Guerri, G.; Messeri, A.; Congedo, L.; Munafo, M. Surface urban heat islands in Italian metropolitan cities: Tree cover and impervious surface influences. *Sci. Total Environ.* **2021**, *751*, 142334. [[CrossRef](#)]
42. Wang, Y.R.; Hensen, D.O.; Samset, B.H.; Stordal, F. Evaluating global and regional land warming trends in the past decades with both MODIS and ERA5-Land land surface temperature data. *Remote Sens. Environ.* **2022**, *280*, 113181. [[CrossRef](#)]
43. Ewing, R.; Rong, F. The impact of urban form on U.S. residential energy use. *Hous. Policy Debate* **2008**, *19*, 1–30. [[CrossRef](#)]
44. Grimm, N.B.; Faeth, S.H.; Golubiewski, N.E.; Redman, C.L.; Wu, J.; Bai, X.; Briggs, J.M. Global Change and the Ecology of Cities. *Science* **2008**, *319*, 756–760. [[CrossRef](#)]
45. Li, H.; Meier, F.; Lee, X.; Chakraborty, T.; Liu, J.; Schaap, M.; Sodoudi, S. Interaction between urban heat island and urban pollution island during summer in Berlin. *Sci. Total Environ.* **2018**, *636*, 818–828. [[CrossRef](#)] [[PubMed](#)]
46. Čeplová, N.; Kalusová, V.; Lososová, Z. Effects of settlement size, urban heat island and habitat type on urban plant biodiversity. *Landsc. Urban Plan.* **2017**, *159*, 15–22. [[CrossRef](#)]
47. Meineke, E.K.; Dunn, R.R.; Frank, S.D. Early pest development and loss of biological control are associated with urban warming. *Biol. Lett.* **2014**, *10*, 20140586. [[CrossRef](#)] [[PubMed](#)]
48. Patz, J.A.; Campbell-Lendrum, D.H.; Holloway, T.; Foley, J.A. Impact of regional climate change on human health. *Nature* **2005**, *438*, 310–317. [[CrossRef](#)]
49. Harlan, S.L.; Brazel, A.J.; Prasad, L.; Stefanov, W.L.; Larsen, L. Neighborhood microclimates and vulnerability to heat stress. *Soc. Sci. Med.* **2006**, *63*, 2847–2863. [[CrossRef](#)]
50. Estoque, R.C.; Murayama, Y.; Myint, S.W. Effects of landscape composition and pattern on land surface temperature: An urban heat island study in the megacities of Southeast Asia. *Sci. Total Environ.* **2017**, *577*, 349–359. [[CrossRef](#)]
51. EPA. *Reducing Urban Heat Islands: Compendium of Strategies*; U.S. Environmental Protection Agency: Washington, DC, USA, 2008.
52. Schwarz, N.; Schlink, U.; Franck, U.; Großmann, K. Relationship of land surface and air temperatures and its implications for quantifying urban heat island indicators—An application for the city of Leipzig (Germany). *Ecol. Indic.* **2012**, *18*, 693–704. [[CrossRef](#)]
53. Arnfield, A.J. Two decades of urban climate research: A review of turbulence, exchanges of energy and water, and the urban heat island. *Int. J. Climatol.* **2003**, *23*, 1–26. [[CrossRef](#)]
54. Sheng, L.; Tang, X.; You, H.; Gu, Q.; Hu, H. Comparison of the urban heat island intensity quantified by using air temperature and Landsat land surface temperature in Hangzhou, China. *Ecol. Indic.* **2017**, *72*, 738–746. [[CrossRef](#)]
55. Ramamurthy, P.; Li, D.; Bou-Zeid, E. High-resolution simulation of heatwave events in New York City. *Theor. Appl. Climatol.* **2015**, *128*, 89–102. [[CrossRef](#)]
56. Fu, P.; Weng, Q.H. A time series analysis of urbanization induced land use and land cover change and its impact on land surface temperature with Landsat imagery. *Remote Sens. Environ.* **2016**, *175*, 205–214. [[CrossRef](#)]
57. Yang, J.; Zhan, Y.X.; Xiao, X.M.; Xia, J.H.C.; Sun, W.; Li, X.M. Investigating the diversity of land surface temperature characteristics in different scale cities based on local climate zones. *Urban Clim.* **2020**, *34*, 100700. [[CrossRef](#)]
58. Qiao, Z.; Tian, G.; Xiao, L. Diurnal and seasonal impacts of urbanization on the urban thermal environment: A case study of Beijing using MODIS data. *ISPRS J. Photogramm. Remote Sens.* **2013**, *85*, 93–101. [[CrossRef](#)]
59. Sun, R.; Lü, Y.; Chen, L.; Yang, L.; Chen, A. Assessing the stability of annual temperatures for different urban functional zones. *Build. Environ.* **2013**, *65*, 90–98. [[CrossRef](#)]
60. Chen, H.C.; Han, Q.; De Vries, B. Modeling the spatial relation between urban morphology, land surface temperature and urban energy demand. *Sustain. Cities Soc.* **2020**, *60*, 102246. [[CrossRef](#)]
61. Zhou, D.; Zhang, L.; Li, D.; Huang, D.; Zhu, C. Climate–vegetation control on the diurnal and seasonal variations of surface urban heat islands in China. *Environ. Res. Lett.* **2016**, *11*, 074009. [[CrossRef](#)]
62. Yang, J.; Ren, J.Y.; Sun, D.Q.; Xiao, X.M.; Xia, J.; Jin, C.; Li, X.M. Understanding land surface temperature impact factors based on local climate zones. *Sustain. Cities Soc.* **2021**, *69*, 102818. [[CrossRef](#)]
63. Song, J.; Du, S.; Feng, X.; Guo, L. The relationships between landscape compositions and land surface temperature: Quantifying their resolution sensitivity with spatial regression models. *Landsc. Urban Plan.* **2014**, *123*, 145–157. [[CrossRef](#)]

64. Rhee, J.; Park, S.; Lu, Z.Y. Relationship between land cover patterns and surface temperature in urban areas. *Gisci. Remote Sens.* **2014**, *51*, 521–536. [[CrossRef](#)]
65. Mohan, M.; Kikegawa, Y.; Gurjar, B.R.; Bhati, S.; Kolli, N.R. Assessment of urban heat island effect for different land use–land cover from micrometeorological measurements and remote sensing data for megacity Delhi. *Theor. Appl. Climatol.* **2013**, *112*, 647–658. [[CrossRef](#)]
66. Yao, L.; Xu, Y.; Zhang, B. Effect of urban function and landscape structure on the urban heat island phenomenon in Beijing, China. *Landsc. Ecol. Eng.* **2019**, *15*, 379–390. [[CrossRef](#)]
67. Unger, J. Connection between urban heat island and sky view factor approximated by a software tool on a 3D urban database. *Int. J. Environ. Pollut.* **2009**, *36*, 59–80. [[CrossRef](#)]
68. Chen, Y.Q.; Shan, B.Y.; Yu, X.W.; Zhang, Q.; Ren, Q.X. Comprehensive effect of the three-dimensional spatial distribution pattern of buildings on the urban thermal environment. *Urban Clim.* **2022**, *46*, 101324. [[CrossRef](#)]
69. de Almeida, C.R.; Teodoro, A.C.; Goncalves, A. Study of the Urban Heat Island (UHI) Using Remote Sensing Data/Techniques: A Systematic Review. *Environments* **2021**, *8*, 105. [[CrossRef](#)]
70. Wan, Z.; Hook, S.; Hulley, G. MODIS/Terra Land Surface Temperature/Emissivity 5-Min L2 Swath 1 km V061. 2021. Available online: <https://ladsweb.modaps.eosdis.nasa> (accessed on 8 February 2023).
71. De Nadai, M.; Xu, Y.Y.; Letouz, E.; Gonzalez, M.C.; Lepri, B. Socio-economic, built environment, and mobility conditions associated with crime: A study of multiple cities. *Sci. Rep.* **2020**, *10*, 12. [[CrossRef](#)]
72. Amani, M.; Ghorbanian, A.; Ahmadi, S.A.; Kakooei, M.; Moghimi, A.; Mirmazloumi, S.M.; Moghaddam, S.H.A.; Mahdavi, S.; Ghahremanloo, M.; Parsian, S.; et al. Google Earth Engine Cloud Computing Platform for Remote Sensing Big Data Applications: A Comprehensive Review. *IEEE J. Sel. Top. Appl. Earth Obs. Remote Sens.* **2020**, *13*, 5326–5350. [[CrossRef](#)]
73. Ma, J.; Cheng, J.C.P.; Jiang, F.F.; Chen, W.W.; Zhang, J.C. Analyzing driving factors of land values in urban scale based on big data and non-linear machine learning techniques. *Land Use Policy* **2020**, *94*, 104537. [[CrossRef](#)]
74. Martinez-Alvarez, F.; Bui, D.T. Advanced Machine Learning and Big Data Analytics in Remote Sensing for Natural Hazards Management. *Remote Sens.* **2020**, *12*, 301. [[CrossRef](#)]
75. Li, Z.C.; Dong, J.W. Big Geospatial Data and Data-Driven Methods for Urban Dengue Risk Forecasting: A Review. *Remote Sens.* **2022**, *14*, 5052. [[CrossRef](#)]
76. Wang, X.; Zhang, Y.; Yu, D.; Qi, J.; Li, S. Investigating the spatiotemporal pattern of urban vibrancy and its determinants: Spatial big data analyses in Beijing, China. *Land Use Policy* **2022**, *119*, 106162. [[CrossRef](#)]
77. Garcia-Palomares, J.C.; Salas-Olmedo, M.H.; Moya-Gomez, B.; Condeco-Melhorado, A.; Gutierrez, J. City dynamics through Twitter: Relationships between land use and spatiotemporal demographics. *Cities* **2018**, *72*, 310–319. [[CrossRef](#)]
78. Laman, H.; Yasmin, S.; Eluru, N. Using location-based social network data for activity intensity analysis: A case study of New York City. *J. Transp. Land Use* **2019**, *12*, 723–740. [[CrossRef](#)]
79. Rizwan, M.; Wan, W.; Cervantes, O.; Gwiazdzinski, L. Using Location-Based Social Media Data to Observe Check-In Behavior and Gender Difference: Bringing Weibo Data into Play. *ISPRS Int. J. Geo-Inf.* **2018**, *7*, 196. [[CrossRef](#)]
80. Wu, C.; Ye, X.; Ren, F.; Du, Q. Check-in behaviour and spatio-temporal vibrancy: An exploratory analysis in Shenzhen, China. *Cities* **2018**, *77*, 104–116. [[CrossRef](#)]
81. Tu, W.; Zhu, T.; Xia, J.; Zhou, Y.; Lai, Y.; Jiang, J.; Li, Q. Portraying the spatial dynamics of urban vibrancy using multisource urban big data. *Comput. Environ. Urban Syst.* **2020**, *80*, 101428. [[CrossRef](#)]
82. Liu, H.; Gong, P.; Wang, J.; Clinton, N.; Bai, Y.; Liang, S. Annual dynamics of global land cover and its long-term changes from 1982 to 2015. *Earth Syst. Sci. Data* **2020**, *12*, 1217–1243. [[CrossRef](#)]
83. Jia, F.X.; Yan, J.F.; Su, F.Z.; Du, J.X.; Zhao, S.Y.; Bai, J.B. Construction of a Scoring Evaluation Model for Identifying Urban Functional Areas Based on Multisource Data. *J. Urban Plan. Dev.* **2022**, *148*, 04022043. [[CrossRef](#)]
84. Tao, Y.; Wang, H.N.; Ou, W.X.; Guo, J. A land-cover-based approach to assessing ecosystem services supply and demand dynamics in the rapidly urbanizing Yangtze River Delta region. *Land Use Policy* **2018**, *72*, 250–258. [[CrossRef](#)]
85. Li, Y.R.; Cao, Z.; Long, H.L.; Liu, Y.S.; Li, W.J. Dynamic analysis of ecological environment combined with land cover and NDVI changes and implications for sustainable urban-rural development: The case of Mu Us Sandy Land, China. *J. Clean. Prod.* **2017**, *142*, 697–715. [[CrossRef](#)]
86. Zeng, C.; Yang, L.D.; Dong, J.N. Management of urban land expansion in China through intensity assessment: A big data perspective. *J. Clean. Prod.* **2017**, *153*, 637–647. [[CrossRef](#)]
87. Li, S.; Wu, C.; Lin, Y.; Li, Z.; Du, Q. Urban Morphology Promotes Urban Vibrancy from the Spatiotemporal and Synergetic Perspectives: A Case Study Using Multisource Data in Shenzhen, China. *Sustainability* **2020**, *12*, 4829. [[CrossRef](#)]
88. Anselin, L. Local Indicators of Spatial Association—Lisa. *Geogr. Anal.* **1995**, *27*, 93–115. [[CrossRef](#)]
89. Anselin, L. *Spatial Econometrics: Methods and Models*; Kluwer Academic Publisher: Dordrecht, The Netherlands, 1988.
90. Anselin, L.; Griffith, D.A. Do spatial effects really matter in regression-analysis. *Pap. Reg. Sci. Assoc.* **1988**, *65*, 11–34. [[CrossRef](#)]
91. Elhorst, J.P. *Spatial Econometrics: From Cross-Sectional Data to Spatial Panels*; Springer: New York, NY, USA, 2014.
92. Yu, D.; Wei, Y.D. Spatial data analysis of regional development in Greater Beijing, China, in a GIS environment. *Pap. Reg. Sci.* **2008**, *87*, 97–117. [[CrossRef](#)]
93. Lu, D.S.; Weng, Q.H. Spectral mixture analysis of ASTER images for examining the relationship between urban thermal features and biophysical descriptors in Indianapolis, Indiana, USA. *Remote Sens. Environ.* **2006**, *104*, 157–167. [[CrossRef](#)]

94. Ma, Y.; Kuang, Y.Q.; Huang, N.S. Coupling urbanization analyses for studying urban thermal environment and its interplay with biophysical parameters based on TM/ETM plus imagery. *Int. J. Appl. Earth Obs. Geoinf.* **2010**, *12*, 110–118. [[CrossRef](#)]
95. Dousset, B.; Gourmelon, F. Satellite multi-sensor data analysis of urban surface temperatures and landcover. *Isprs J. Photogramm. Remote Sens.* **2003**, *58*, 43–54. [[CrossRef](#)]
96. Yang, Q.Q.; Huang, X.; Tang, Q.H. The footprint of urban heat island effect in 302 Chinese cities: Temporal trends and associated factors. *Sci. Total Environ.* **2019**, *655*, 652–662. [[CrossRef](#)]
97. Anselin, L. Lagrange Multiplier Test Diagnostics for Spatial Dependence and Spatial Heterogeneity. *Geogr. Anal.* **1988**, *20*, 1–17. [[CrossRef](#)]
98. Anselin, L.; Bera, A.K.; Florax, R.; Yoon, M.J. Simple diagnostic tests for spatial dependence. *Reg. Sci. Urban Econ.* **1996**, *26*, 77–104. [[CrossRef](#)]
99. R Core Team. *R: A Language and Environment for Statistical Computing*; R Foundation for Statistical Computing: Vienna, Austria, 2019.
100. Bivand, R.; Piras, G. Comparing Implementations of Estimation Methods for Spatial Econometrics. *J. Stat. Softw.* **2015**, *63*, 36. [[CrossRef](#)]
101. Bivand, R.; Millo, G.; Piras, G. A Review of Software for Spatial Econometrics in R. *Mathematics* **2021**, *9*, 1276. [[CrossRef](#)]
102. Qiao, Z.; Liu, L.; Qin, Y.W.; Xu, X.L.; Wang, B.W.; Liu, Z.J. The Impact of Urban Renewal on Land Surface Temperature Changes: A Case Study in the Main City of Guangzhou, China. *Remote Sens.* **2020**, *12*, 794. [[CrossRef](#)]
103. Chase, J.; Crawford, M.; Kaliski, J. *Everyday Urbanism: Expanded*; The Monacelli Press: New York, NY, USA, 2008; p. 224.
104. Alawadi, K.; Hashem, S.; Maghelal, P. Perspectives on Everyday Urbanism: Evidence from an Abu Dhabi Neighborhood. *J. Plan. Educ. Res.* **2023**, *43*, 0739456X221097839. [[CrossRef](#)]
105. Zhou, W.Q.; Huang, G.L.; Cadenasso, M.L. Does spatial configuration matter? Understanding the effects of land cover pattern on land surface temperature in urban landscapes. *Landsc. Urban Plan.* **2011**, *102*, 54–63. [[CrossRef](#)]
106. Long, Y.; Han, H.Y.; Tu, Y.C.; Shu, X.F. Evaluating the effectiveness of urban growth boundaries using human mobility and activity records. *Cities* **2015**, *46*, 76–84. [[CrossRef](#)]
107. Xie, Z.W.; Ye, X.Y.; Zheng, Z.H.; Li, D.; Sun, L.S.; Li, R.R.; Benya, S. Modeling Polycentric Urbanization Using Multisource Big Geospatial Data. *Remote Sens.* **2019**, *11*, 310. [[CrossRef](#)]

Disclaimer/Publisher’s Note: The statements, opinions and data contained in all publications are solely those of the individual author(s) and contributor(s) and not of MDPI and/or the editor(s). MDPI and/or the editor(s) disclaim responsibility for any injury to people or property resulting from any ideas, methods, instructions or products referred to in the content.